



3 4456 0515411 4

ORNL-4807

Cy1

CENTRAL RESEARCH LIBRARY

(ENDF-198)

NATURAL NICKEL AND ⁶⁰Ni NEUTRON ELASTIC AND INELASTIC SCATTERING CROSS SECTIONS FROM 4.07 TO 8.56 MeV

W. E. Kinney
F. G. Perey

OAK RIDGE NATIONAL LABORATORY
CENTRAL RESEARCH LIBRARY
DOCUMENT COLLECTION

LIBRARY LOAN COPY

DO NOT TRANSFER TO ANOTHER PERSON

If you wish someone else to see this document, send it along with document and the library will arrange a loan.

LC-7500
10-1975



OAK RIDGE NATIONAL LABORATORY

OPERATED BY UNION CARBIDE CORPORATION • FOR THE U.S. ATOMIC ENERGY COMMISSION

Printed in the United States of America. Available from
National Technical Information Service
U.S. Department of Commerce
5285 Port Royal Road, Springfield, Virginia 22151
Price: Printed Copy \$4.00; Microfiche \$0.95

This report was prepared as an account of work sponsored by the United States Government. Neither the United States nor the United States Atomic Energy Commission, nor any of their employees, nor any of their contractors, subcontractors, or their employees, makes any warranty, express or implied, or assumes any legal liability or responsibility for the accuracy, completeness or usefulness of any information, apparatus, product or process disclosed, or represents that its use would not infringe privately owned rights.

ORNL-4807
UC-79d
(ENDF-198)

Contract No. W-7405-eng-26

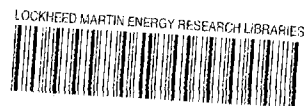
Neutron Physics Division

NATURAL NICKEL AND ^{60}Ni NEUTRON ELASTIC AND INELASTIC
SCATTERING CROSS SECTIONS FROM 4.07 TO 8.56 MeV

W. E. Kinney and F. G. Perey

JANUARY 1974

OAK RIDGE NATIONAL LABORATORY
Oak Ridge, Tennessee 37830
operated by
UNION CARBIDE CORPORATION
for the
U.S. ATOMIC ENERGY COMMISSION



3 4456 0515411 4

CONTENTS

Abstract	1
Introduction.....	1
Data Acquisition.....	1
Data Reduction	2
Results	3
The Isotopes of Natural Nickel	3
Elastic Scattering Differential Cross Sections.....	5
Inelastic Scattering Differential Cross Sections.....	13
Excitation Functions	13
Inelastic Scattering to the Continuum.....	17
Conclusions.....	22
Acknowledgments	22
References.....	23
Appendix	25

NATURAL NICKEL AND ^{60}Ni NEUTRON ELASTIC AND INELASTIC SCATTERING CROSS SECTIONS FROM 4.07 TO 8.56 MeV

W. E. Kinney and F. G. Perey

ABSTRACT

Measured neutron elastic and inelastic scattering cross sections for natural nickel between 4.07 and 8.56 MeV are presented and compared with the elastic differential cross sections of Holmqvist and Wiedling and with ENDF/B III MAT 1123. Our elastic differential cross sections are in general agreement with those of Holmqvist and Wiedling but our angle-integrated differential elastic cross sections are systematically higher by about 10% than those of Holmqvist and Wiedling above 4.6 MeV, a situation found in comparing the two sets of data for other elements. The ENDF/B III MAT 1123 elastic angular distributions are found to be in poor agreement with experimental results from 4 to 8.5 MeV though the ENDF/B III MAT 1123 angle-integrated differential elastic cross sections agree generally within experimental uncertainties with our results over this energy range. Additional measurements of ^{60}Ni neutron elastic and inelastic scattering cross sections at 4.34 and 4.92 MeV are given and compared with our previous results from 6 to 8.5 MeV and with our natural nickel results. Agreement is shown to be excellent. Inelastic scattering cross sections to the 1.450 MeV level in ^{58}Ni are computed from the natural nickel and ^{60}Ni data. An evaporation model of inelastic scattering to levels of excitation energy in the residual nucleus below 6 MeV is found to be of questionable validity.

INTRODUCTION

The data reported here are the results of one of a series of experiments to measure neutron elastic and inelastic scattering cross sections at the ORNL Van de Graaffs. Reports in the series are listed in Reference 1. This report presents measured neutron elastic and inelastic scattering cross sections for natural nickel at 11 energies between 4.07 and 8.56 MeV and ^{60}Ni at six energies between 4.07 and 5.50 MeV. To assist in the evaluation of the data, the data acquisition and reduction techniques are first briefly discussed. For the purposes of discussion the data are presented in graphical form and are compared with the results of Holmqvist and Wiedling² and with ENDF/B III (Evaluated Neutron Data File B, Version III) MAT 1123. Tables of numerical values of the elastic scattering cross sections and cross sections for inelastic scattering to discrete levels in the residual nucleus are given in an appendix.

DATA ACQUISITION

The data were obtained with conventional time-of-flight techniques. Pulsed (2 MHz), bunched (approximately 1.5 nsec full width at half maximum, FWHM) deuterons

accelerated by the ORNL Van de Graaffs interacted with deuterium in a gas cell to produce neutrons by the $D(d,n)^3\text{He}$ reaction. The gas cells, of length 1 and 2 cm, were operated at pressures of approximately 1.5 atm and gave neutron energy resolutions of the order of ± 60 keV.

The neutrons were scattered from a solid right circular cylindrical sample of natural nickel, 1.52 cm diameter, 2.58 cm high of mass 41.86 gm and placed approximately 10 cm from the gas cells when the detector angles were greater than 25 degrees. For smaller detector angles the cell-to-sample distance had to be increased to 33 cm in order to shield the detectors from neutrons coming directly from the gas cells. The ^{60}Ni sample was a solid right circular cylinder of metallic ^{60}Ni (greater than 99.9% ^{60}Ni) of diameter 1.76 cm, height 2.62 cm, and mass 35.68 gm.

The scattered neutrons were detected by 12.5 cm diameter NE-213 liquid scintillators optically coupled to XP-1040 photomultipliers. The scintillators were 2.5 cm thick. Data at three angles were taken simultaneously with detectors equally spaced at 7.5 deg. intervals. Flight paths were approximately 5 m with the detector angles ranging from 15 to 140 degrees. The gas cell neutron production was monitored by a time-of-flight system which used a 5 cm diameter by 2.5 cm thick NE-213 scintillator viewed by a 56-AVP photomultiplier placed about 4 m from the cell at an angle of 55 degrees with the incident deuteron beam.

For each event a PDP-7 computer was given the flight time of a detected recoil proton event with reference to a beam pulse signal, the pulse height of the recoil proton event, and identification of the detector. The electronic equipment for supplying this information to the computer consisted, for the most part, of standard commercial components. The electronic bias was set at approximately 700 keV neutron energy to ensure good pulse shape discrimination against gamma-rays at all energies.

The detector efficiencies were measured by (n,p) scattering from a 6 mm diameter polyethylene sample and by detecting source $D(d,n)^3\text{He}$ neutrons at 0 degrees³. Both interactions gave results which agreed with each other and which yielded efficiency versus energy curves that compared well with calculations⁴.

DATA REDUCTION

Central to the data reduction process was the use of a light pen with the PDP-7 computer oscilloscope display programs to extract peak areas from spectra. The light pen made a comparatively easy job of estimating errors in the cross section caused by extreme but possible peak shapes.

The reduction process started on an IBM-360 by normalizing a sample-out to a sample-in time-of-flight spectrum by the ratio of their monitor neutron peak areas, subtracting the sample-out spectrum, and transforming the difference spectrum into a spectrum of center-of-mass cross section versus excitation energy. This transformation allowed ready comparison of spectra taken at different angles and incident neutron energies by removing kinematic effects. It also made all single peaks have approximately the same shape and width regardless of excitation energy (in a time-of-flight spectrum, single peaks broaden with increasing flight time). A spectrum of the variance based on the counting

statistics of the initial data was also computed. Figure 1 shows a typical time-of-flight spectrum and its transformed energy spectrum.

The transformed spectra were read from magnetic tape written by the IBM-360 into the PDP-7 computer and the peak stripping was done with the aid of the light pen. A peak was stripped by drawing a background beneath it, subtracting the background, and calculating the area, centroid, and FWHM of the difference. The variance spectrum was used to compute a counting statistics variance corresponding to the stripped peak. Peak stripping errors due to uncertainties in the residual background under the peaks or to the tails of imperfectly resolved nearby peaks could be included with the other errors by stripping the peaks several times corresponding to high, low, and best estimates of this background. Although somewhat subjective, the low and high estimates of the cross sections were identified with 95% confidence limits; these, together with the best estimate, defined upper and lower errors due to stripping. When a spectrum was completely stripped, the output information was written on magnetic tape for additional processing by the IBM-360.

Finite sample corrections were performed according to semianalytic recipes whose constants were obtained from fits to Monte Carlo results⁵. The corrections were 6 - 14% at forward angles, 40 - 70% in the first minimum, and 14 - 17% on the second maximum.

The final error analysis included uncertainties in the geometrical parameters (scatterer size, gas cell-to-scatterer distance, flight paths, etc.) and uncertainties in the finite sample corrections.

The measured differential elastic scattering cross sections were fitted by least squares to a Legendre series:

$$\sigma(\mu = \cos\theta) = \sum [(2k+1)/2] a_k P_k(\mu)$$

the points being weighted by the inverse of their variances which were computed by squaring the average of the upper and lower uncertainties. The common 7% uncertainty in absolute normalization was not included in the variances for the fitting. In order to prevent the fit from giving totally unrealistic values outside the angular range of our measurements, we resorted to the inelegant but workable process of adding three points equally spaced in angle between the largest angle of measurement and 175 degrees. The differential cross sections at the added points were chosen to approximate the diffraction pattern at large angles, but were assigned 50% errors.

RESULTS

The Isotopes of Natural Nickel

Natural nickel contains 5 isotopes with natural abundances⁶: 67.76% ⁵⁸Ni, 26.16% ⁶⁰Ni, 1.25% ⁶¹Ni, 3.66% ⁶²Ni, and 1.16% ⁶⁴Ni. Inelastic scattering to the 0.0674 and 0.284 MeV levels in ⁶¹Ni was not separated from elastic scattering with our resolution but because of the low natural abundance of ⁶¹Ni the contribution is negligible. The first excited states of ⁶²Ni and ⁶⁴Ni have excitation energies of 1.172 and 1.34 MeV, respectively, and inelastic scattering to these levels is included in the natural nickel inelastic scattering to the 1.45 MeV level in ⁵⁸Ni and to the 1.332 MeV level in ⁶⁰Ni.

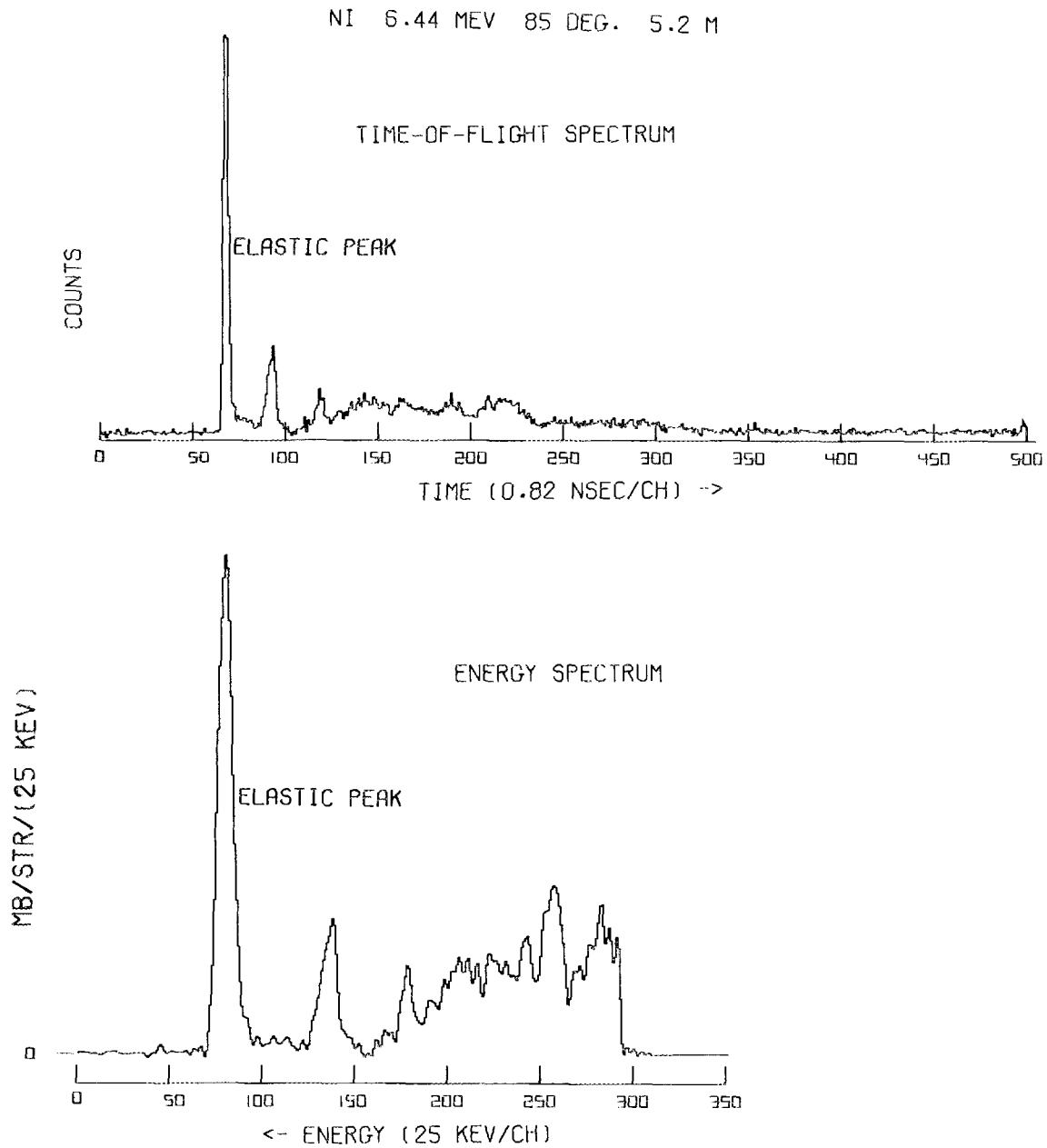


Fig. 1. A typical time-of-flight spectrum for natural nickel with its transformed energy spectrum. The data were taken at 6.44 MeV incident neutron energy at 85 degrees with a 5.2 m flight path. The sample-out spectrum has not been subtracted from the time-of-flight spectrum. Note that the energy spectrum has been offset to allow negative excursions due to statistics in the subtraction of the sample-out. The energy spectrum terminates at approximately 1 MeV scattered neutron energy - very nearly channel 350 in the time-of-flight spectrum. The large peak to the left of both spectra is the elastic peak.

Elastic Scattering Differential Cross Sections

Natural Nickel

Our differential elastic scattering cross sections for natural nickel are shown in Figure 2 with Legendre fits to the data. Wick's Limit is shown and was used in the fitting.

Figures 3 and 4 compare our differential elastic scattering cross sections with those of Holmqvist and Wiedling (H+W)². The angular distributions of ENDF/B III MAT 1123 normalized to the integrals of the experimental differential elastic scattering cross sections are also shown in the figures. The two sets of experimental data appear to be consistent so far as shapes are concerned with the first minimum falling at about the same angle in both sets and slowly moving toward smaller angles with increasing energy.

The ENDF/B III MAT 1123 angular distributions are generally in poor agreement with experimental results. The forward peak is poorly described and the ENDF/B first minima lie roughly 15 degrees beyond the experimental first minima. ENDF/B MAT 1123 uses a Legendre series of order 16 to describe the elastic angular distributions while the maximum order needed to fit the experimental distributions is 9. The use of a Legendre series of order larger than necessary often introduces unphysical structure into angular distributions and needlessly complicates the application of an ENDF/B evaluation.

The degree of agreement among our elastic differential cross sections and those of Holmqvist and Wiedling might be estimated with the help of Figures 5 and 6 where normalized Legendre expansion coefficients ($a_0 = 1$) resulting from fits to both sets of data are plotted as a function of incident neutron energy. The curves are quadratic least-squares fits to both sets of data with the resulting coefficients given in the figures. The Legendre coefficients resulting from fits to our data are uniformly higher than those resulting from fits to the data of Holmqvist and Wiedling. The somewhat higher contribution of all the Legendre Polynomials in the fits to our data implies somewhat more structure, i.e. larger ratios of maxima to minima, in our data than in the data of Holmqvist and Wiedling. This indeed seems to be the case upon closer inspection of Figures 3 and 4. About equal numbers of coefficients from each set of data lie outside one standard deviation of the curve fitting both sets. Until, if ever, a preference for one set of data over another can be established, the quadratic fits to both sets should offer the best experimental description to date of neutron elastic scattering angular distributions on natural nickel from 4 to 8.56 MeV.

⁶⁰Ni

Our recently measured ⁶⁰Ni differential elastic scattering cross sections at 4.34 and 4.92 MeV are shown in Figure 7 with our previously reported results (PLK)¹ at higher energies. Legendre fits to the data are shown. WICK indicates Wick's Limit and was used in fitting the 4.34 and 4.92 MeV data.

Elastic scattering from natural nickel and ⁶⁰Ni should be about the same both in magnitude and in angular distributions. Our elastic differential cross sections for both natural nickel and ⁶⁰Ni are compared in Figure 8 where it is seen agreement is excellent.

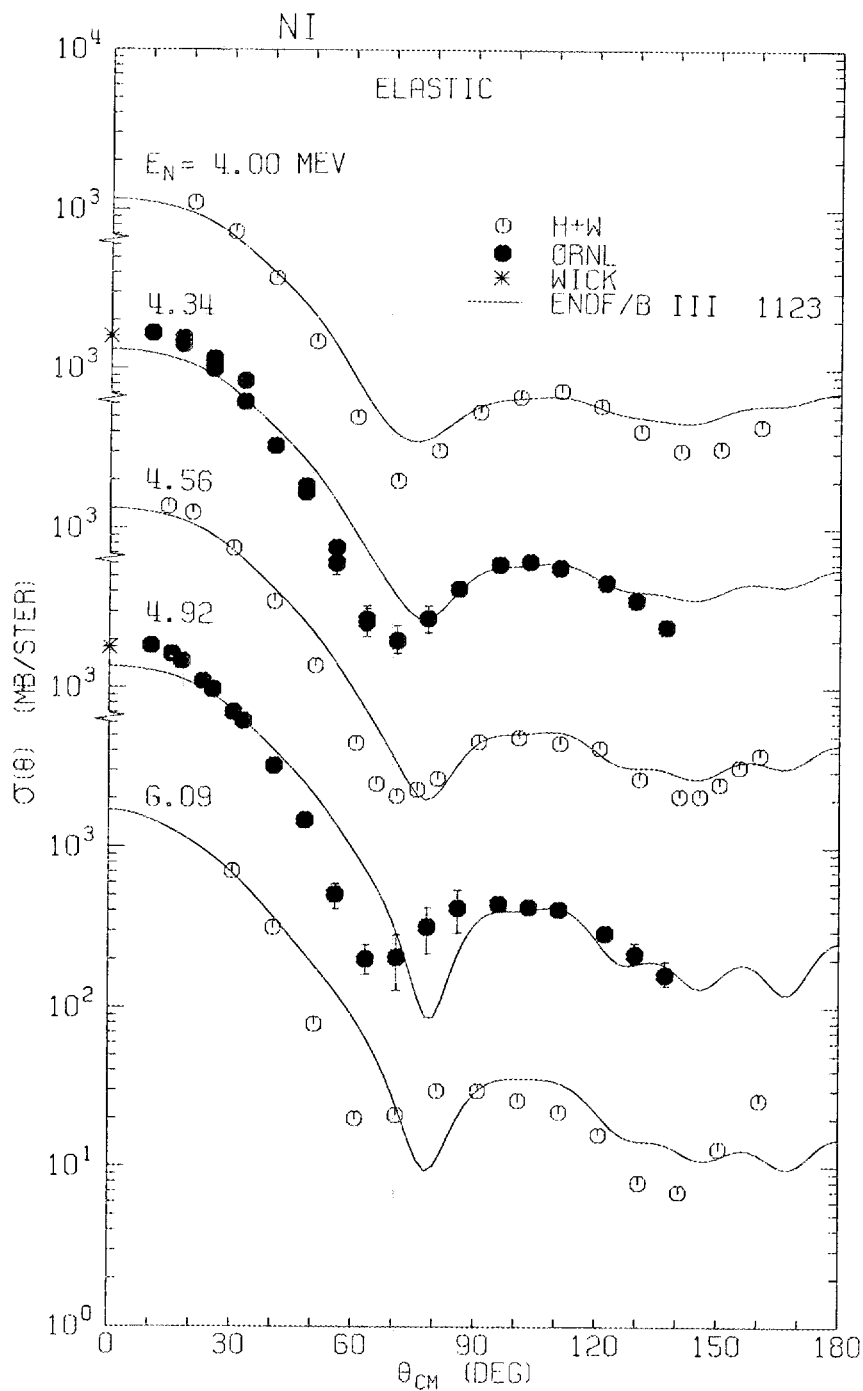


Fig. 3. Our natural nickel neutron differential elastic center-of-mass cross sections compared with the data of Holmqvist and Wiedling $(H+W)^2$ and with the angular distributions of ENDF/B III MAT 1123 from 4.00 to 6.09 MeV. WICK indicates Wick's Limit. The 7% uncertainty in absolute normalization common to all points is not included in the error bars.

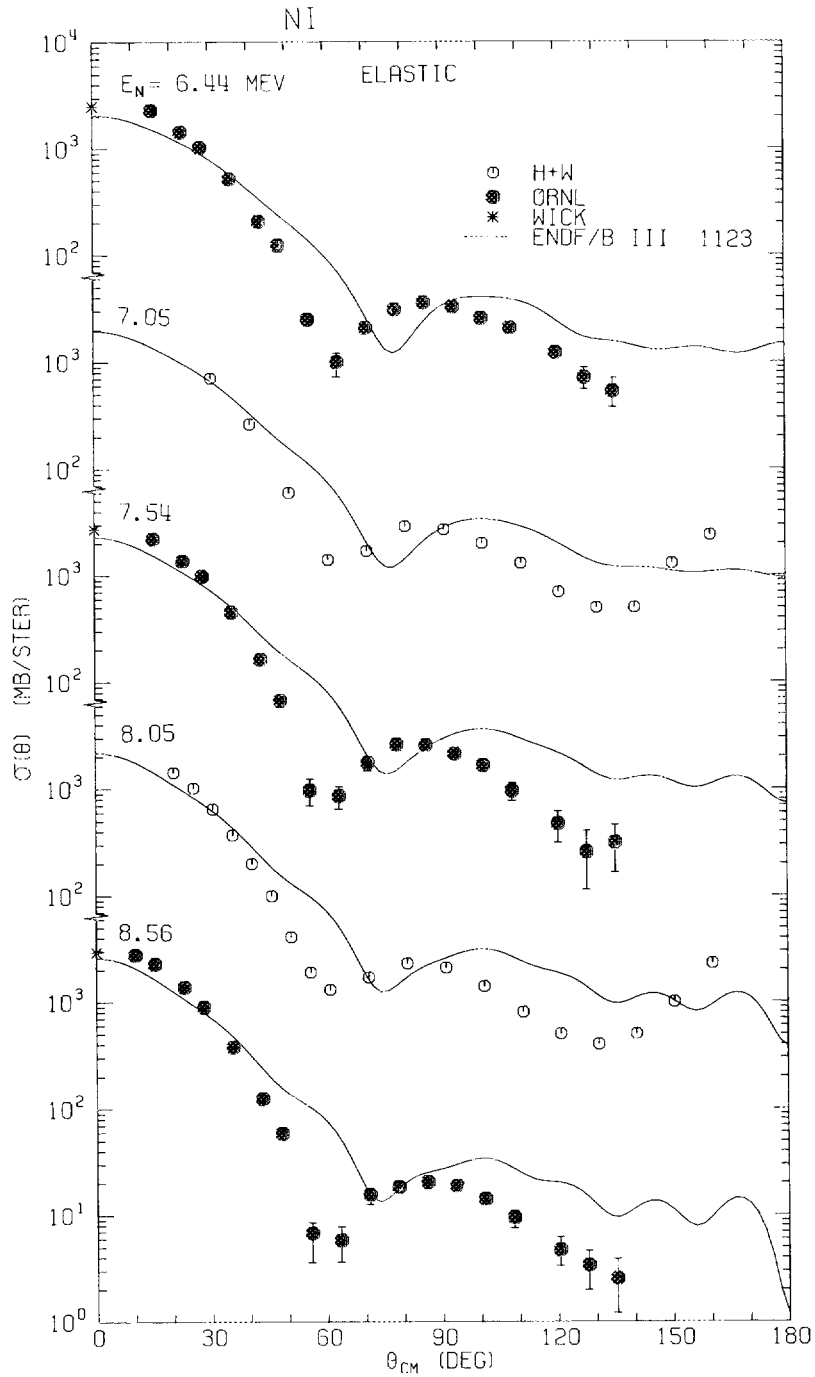


Fig. 4. Our natural nickel neutron differential elastic center-of-mass cross sections compared with the data of Holmqvist and Wiedling (H+W)² and with the angular distributions of ENDF/B III MAT 1123 from 6.44 to 8.56 MeV. WICK indicates Wick's Limit. The 7% uncertainty in absolute normalization common to all points is not included in the error bars.

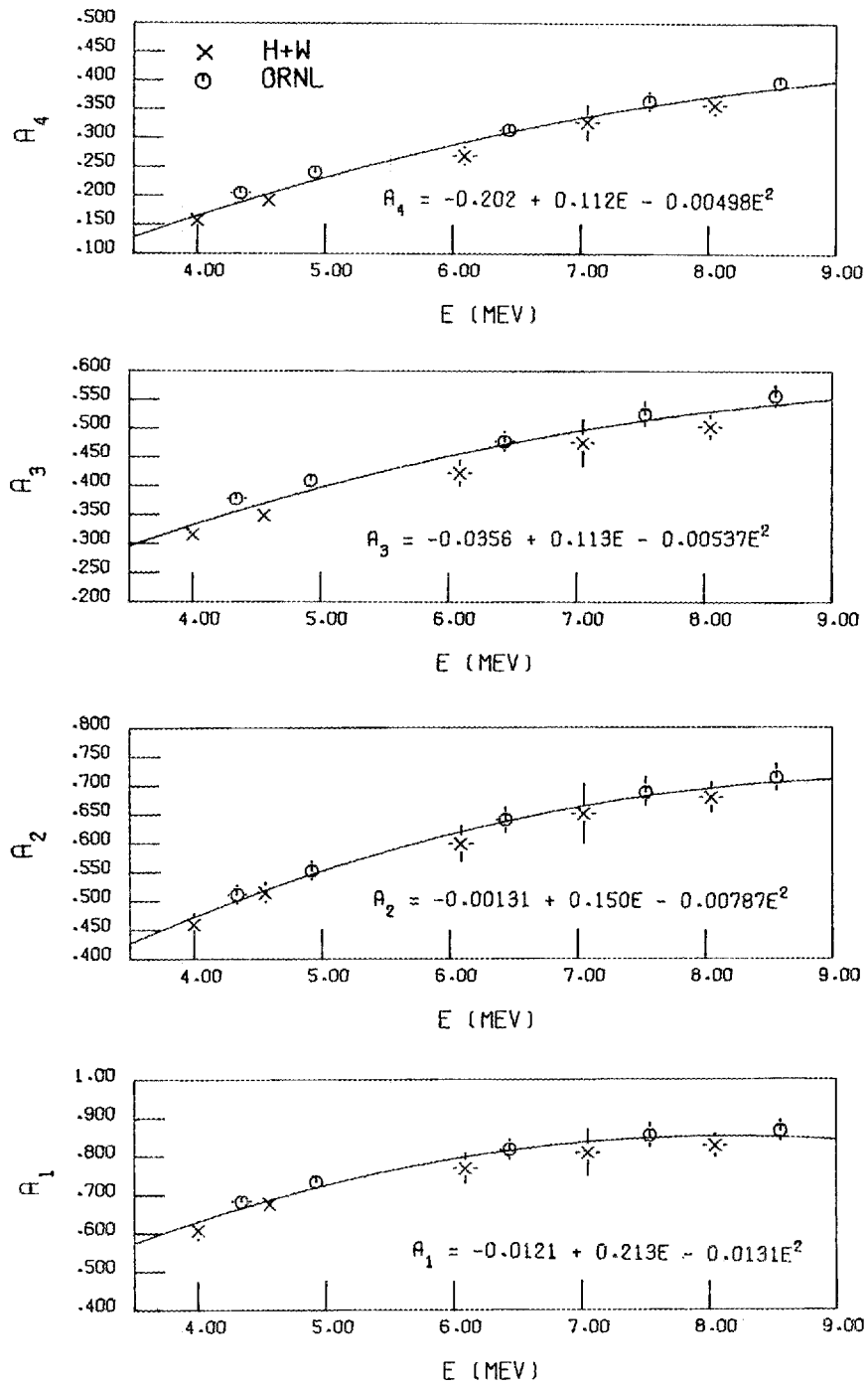


Fig. 5. The first through fourth normalized Legendre expansion coefficients obtained by fitting the natural nickel differential elastic scattering cross sections of Holmqvist and Wiedling and our data as a function of incident neutron energy, E. The curves result from quadratic least squares fits to both sets of data with constants given in the equations.

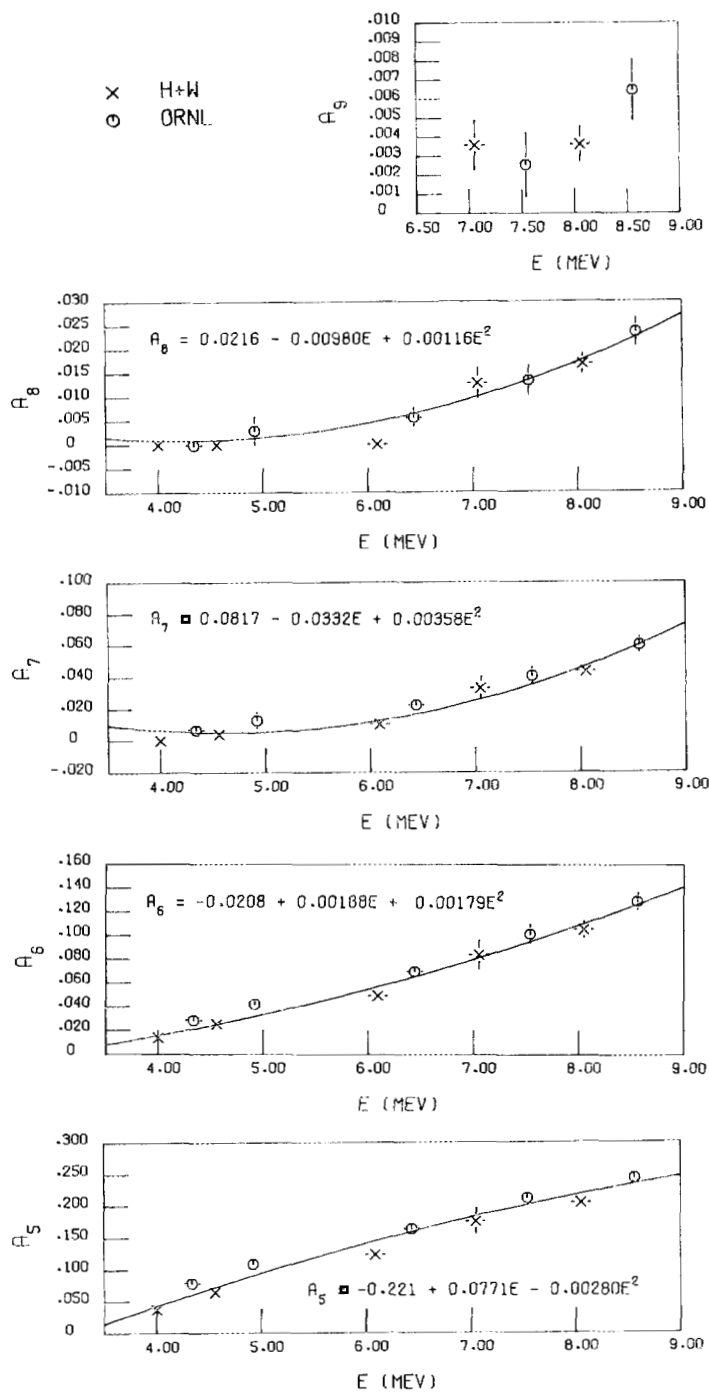


Fig. 6. The fifth through ninth normalized Legendre expansion coefficients obtained by fitting the natural nickel differential neutron elastic scattering cross sections of Holmqvist and Wiedling² and our data as a function of incident neutron energy, E. The curves result from quadratic least squares fits to both sets of data with constants given in the equations.

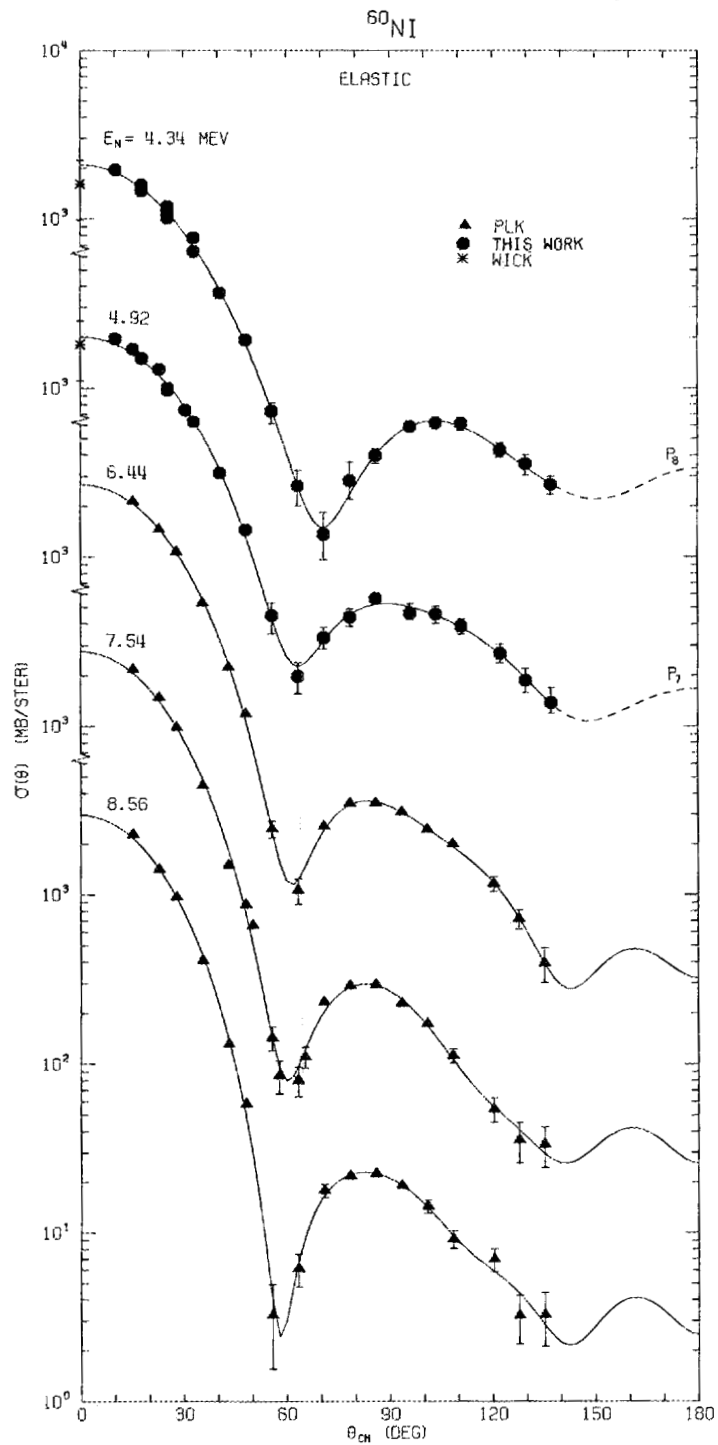


Fig. 7. Our currently reported ^{60}Ni neutron differential elastic center-of-mass scattering cross sections at 4.34 and 4.92 MeV together with our previously reported values (PLK)¹ and Legendre fits to the data. WICK indicates Wick's Limit. The 7% uncertainty common to all points is not included in the error bars.

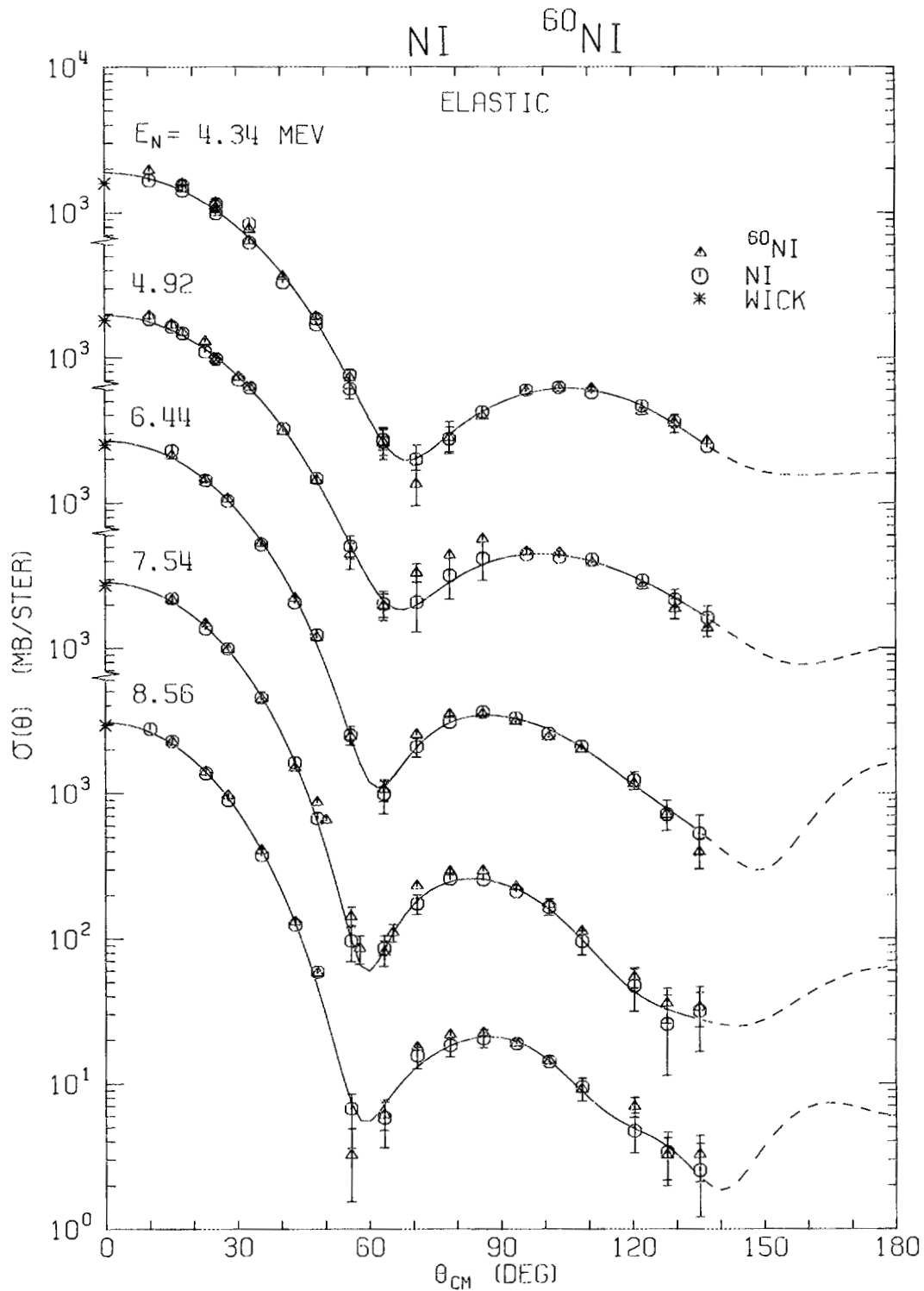


Fig. 8. A comparison of our natural nickel and ^{60}Ni neutron differential elastic center-of-mass scattering cross sections with least squares Legendre fits to the natural nickel data.

Inelastic Scattering Differential Cross Sections

Natural Nickel

Meaningful inelastic scattering cross sections could be extracted only for inelastic scattering to levels in ^{58}Ni and ^{60}Ni with the natural nickel sample since the isotopic abundances of the other isotopes are so small. Figure 9 shows our differential cross sections per atom of natural nickel for inelastic scattering to the 1.333 MeV level in ^{60}Ni and the 1.450 MeV level in ^{58}Ni . These are both 2^+ levels and the angular distributions of inelastic scattering to the levels might be expected to be asymmetric about 90 deg. due to the effect of direct interactions. Indeed, the normalized values of the coefficients of the first and third Legendre Polynomials in the Legendre least squares fits to the data increase from 0.09 and -0.0057 , respectively, at 4.92 MeV to 0.2 and 0.03, respectively, at 8.56 MeV while the normalized value of the coefficient of the second Legendre Polynomial stays roughly constant around 0.05 (See Appendix).

At incident neutron energies other than 4.34, 4.92, 6.44, 7.54, and 8.56 MeV data were taken at three angles only. Values of the angle-integrated cross sections for inelastic scattering to the 1.333 MeV level in ^{60}Ni and to the 1.450 MeV level in ^{58}Ni in natural nickel at these energies were corrected for anisotropy by

- 1) linearly interpolating the normalized Legendre coefficient resulting from the fits to the measured differential cross sections at adjacent energies for which more complete angular distributions were measured, and
- 2) adjusting the magnitudes of the interpolated Legendre coefficients to give a reasonable fit to the data at the three angles.

ENDF/B III MAT 1123 assumes that the angular distributions of all inelastically scattered neutrons are isotropic.

^{60}Ni

Our recently measured differential scattering cross sections for inelastic scattering to the 1.333 MeV level in ^{60}Ni are shown in Figure 10 with our previously reported data (PLK)¹. Anisotropy in the angular distributions is not evident at 4.34 and 4.92 MeV but becomes so at the higher energies.

Excitation Functions

Our angle-integrated differential cross sections per atom of natural nickel are shown as a function of energy in Figure 11. The data of Holmqvist and Wiedling (H+W)² are also shown together with the curve from ENDF/B III MAT 1123.

Our data appear to be in agreement with that of Holmqvist and Wiedling below 5 MeV but at higher energies our data are systematically approximately 200 mb higher, roughly 10%, than that of Holmqvist and Wiedling, though the error bars of interpolated values overlap. We find a similar situation in comparing our chromium and copper data with that of Holmqvist and Wiedling¹. Holmqvist and Wiedling used the T(p,n)³He

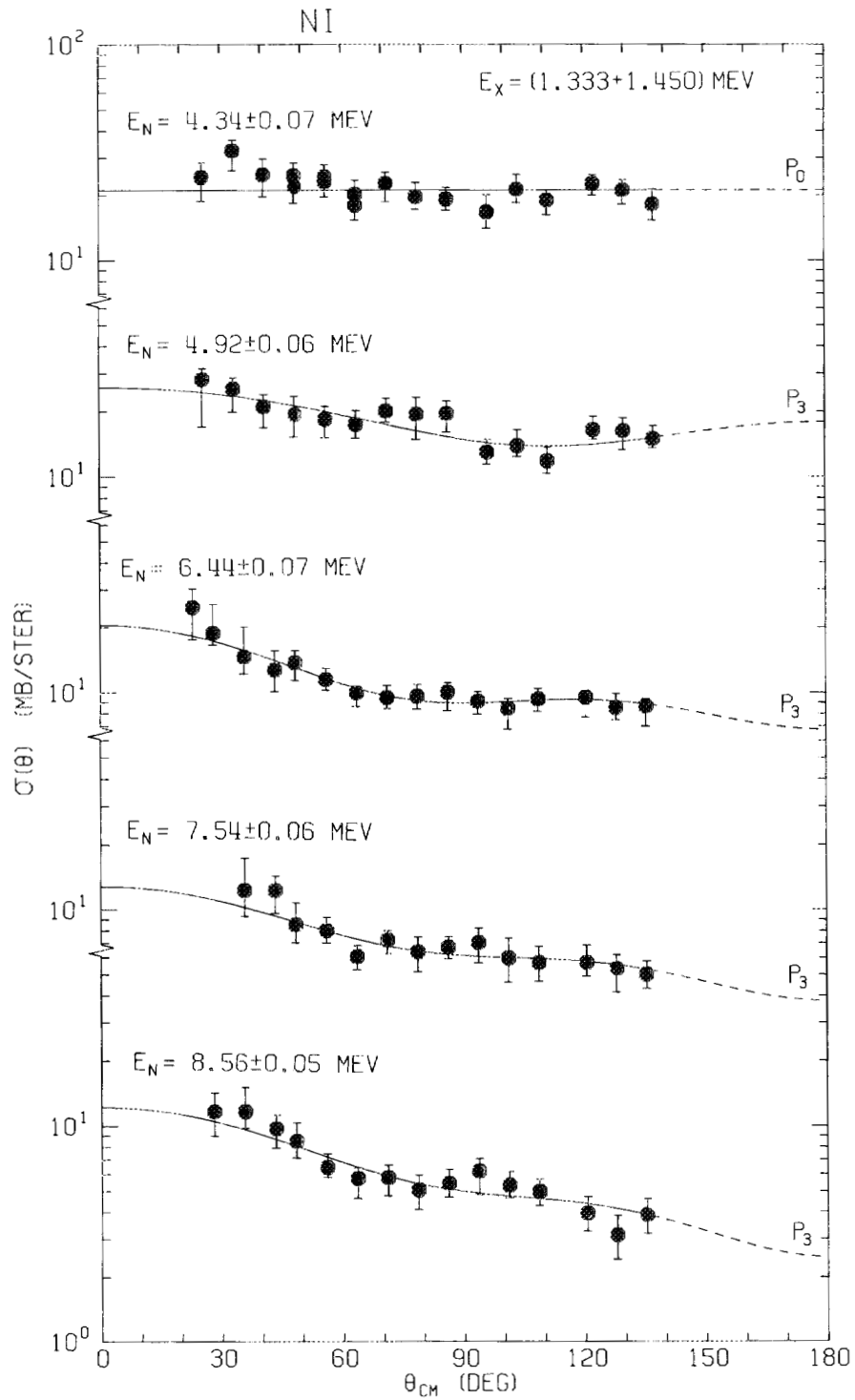


Fig. 9. Our differential center-of-mass cross sections per atom of natural nickel for combined neutron inelastic scattering to the 1.333 MeV level in ^{60}Ni and to the 1.450 MeV level in ^{58}Ni . The curves are least squares Legendre fits to the data.

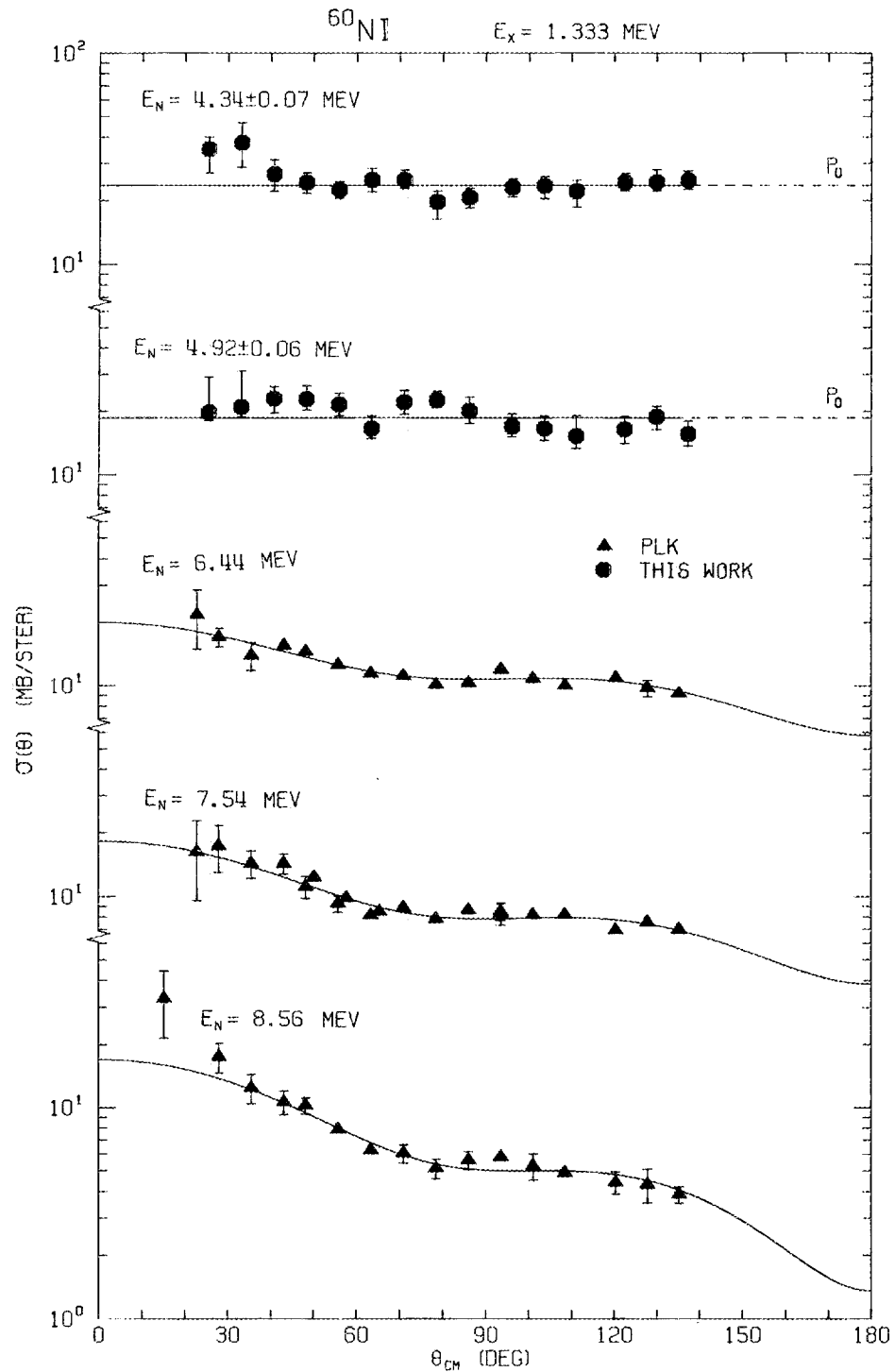


Fig. 10. Our differential center-of-mass cross sections for neutron inelastic scattering to the 1.333 MeV level in ^{60}Ni . The cross sections are per atom of ^{60}Ni . The curves result from least squares Legendre fits to the data.

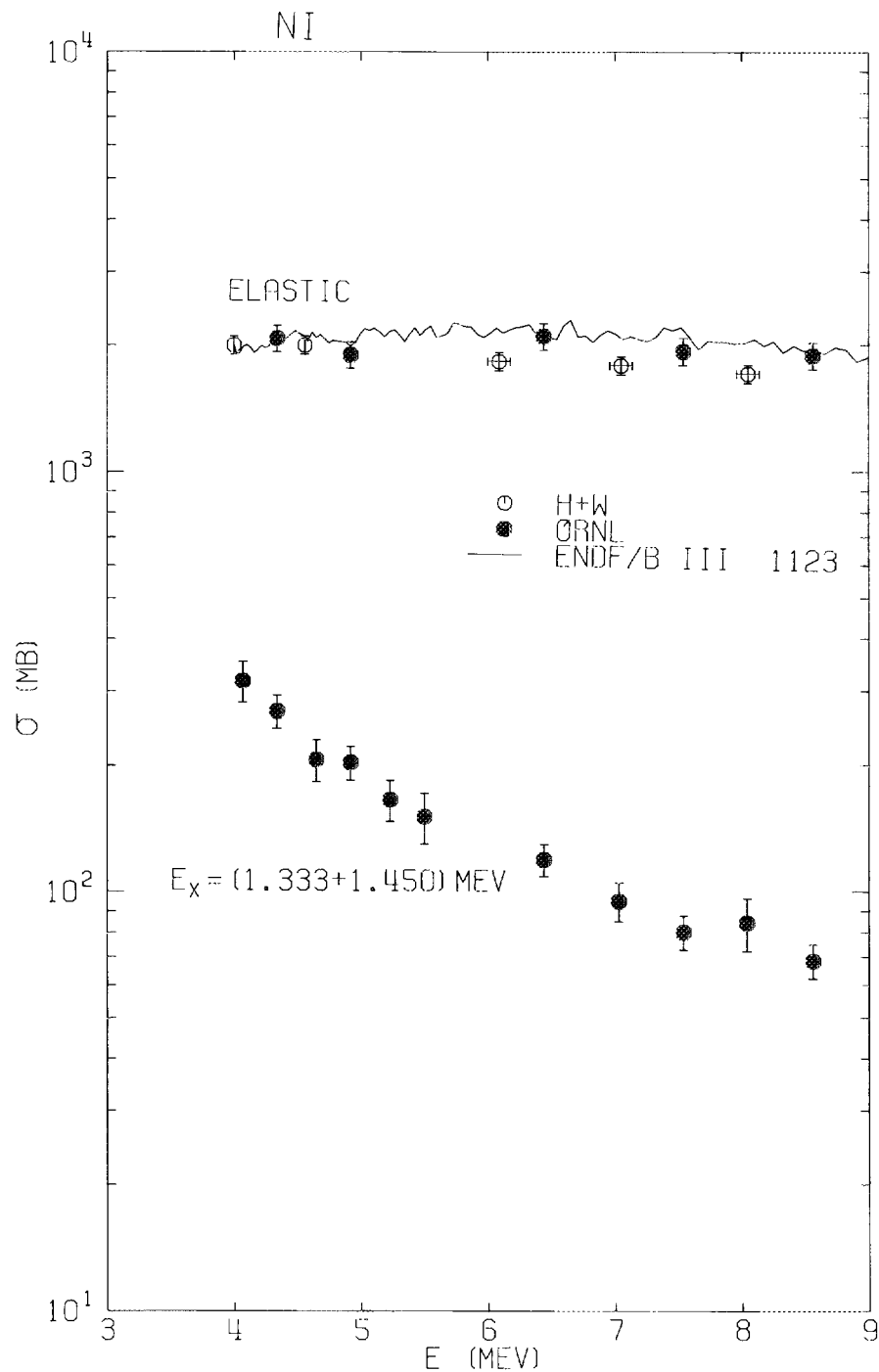


Fig. 11. Our angle-integrated cross sections for neutron elastic scattering on natural nickel and cross sections per atom of natural nickel for inelastic scattering to both the 1.333 MeV level in ^{60}Ni and the 1.450 MeV level in ^{58}Ni as a function of incident neutron energy. Elastic data of Holmqvist and Wiedling (H+W)² are shown. The curve is from ENDF/B III MAT 1123.

reaction to produce neutrons of energies less than 4.6 MeV. To produce neutrons of higher energies, they used the $D(d,n)^3\text{He}$ reaction. Our neutrons were always produced by the $D(d,n)^3\text{He}$ reaction but we used a 3 MeV Van de Graaff to produce neutrons of energies less than 5.5 MeV and used a 5.5 MeV Van de Graaff to produce neutrons of energies greater than 5.5 MeV. Our data taken on both accelerators at nearly the same incident neutron energy are in agreement¹, e.g. ^{54}Fe and natural iron at 5.5 MeV. Deuterons striking beam tubing, collimators, and target structure give rise to higher backgrounds than do protons. An overestimate of backgrounds might possibly explain some of the differences in the two sets of data.

The ENDF/B III MAT 1123 curve lies within experimental uncertainties of all our data save the point at 7.54 MeV and clearly is in better agreement with our higher values than with those of Holmqvist and Wiedling. ENDF/B III MAT 1123 cuts off all its inelastic scattering to discrete levels in the isotopes of natural nickel at an incident neutron energy of 4 MeV and relies on inelastic scattering to a continuum above this energy using an evaporation model with a constant nuclear "temperature" of 1 MeV.

A comparison is made in Figure 12 of our angle-integrated differential cross sections for ^{60}Ni and natural nickel as a function of incident neutron energy. The angle-integrated differential cross sections *per atom of natural nickel* for inelastic scattering to the 1.333 MeV level in ^{60}Ni are shown together with the angle-integrated cross sections per atom of natural nickel for scattering to the 1.450 MeV level in ^{58}Ni obtained by subtracting the ^{60}Ni inelastic data from the data for natural nickel for inelastic scattering to these two levels in the respective isotopes. These data are given in Table I.

Table I. Angle-integrated differential cross sections per atom of natural nickel for inelastic scattering to the 1.333 MeV level in ^{60}Ni and to the 1.450 MeV level in ^{58}Ni .

E_n , MeV	$\sigma_{1.333}^{60}\text{Ni}$	$\sigma_{1.450}^{58}\text{Ni}$
4.34 ± 0.07	77 ± 6 mb	188 ± 28 mb
4.92 ± 0.06	61 ± 5 mb	155 ± 23 mb
6.44 ± 0.07	38 ± 3 mb	94 ± 14 mb
7.54 ± 0.06	29 ± 2 mb	56 ± 10 mb
8.56 ± 0.05	21 ± 2 mb	51 ± 7 mb

Inelastic Scattering to the Continuum

The rapidly increasing density of levels in the isotopes of natural nickel above an excitation energy of 2 MeV, particularly in ^{60}Ni , produced inelastically scattered neutron spectra which we reduced as inelastic scattering to a structured "continuum" of final states rather than attempting to extract cross sections for inelastic scattering to groups of levels or to bands of excitation energy. Figure 13 shows our "continuum" inelastic scattering data where our angle-averaged double-differential cross sections for scattering to an excitation

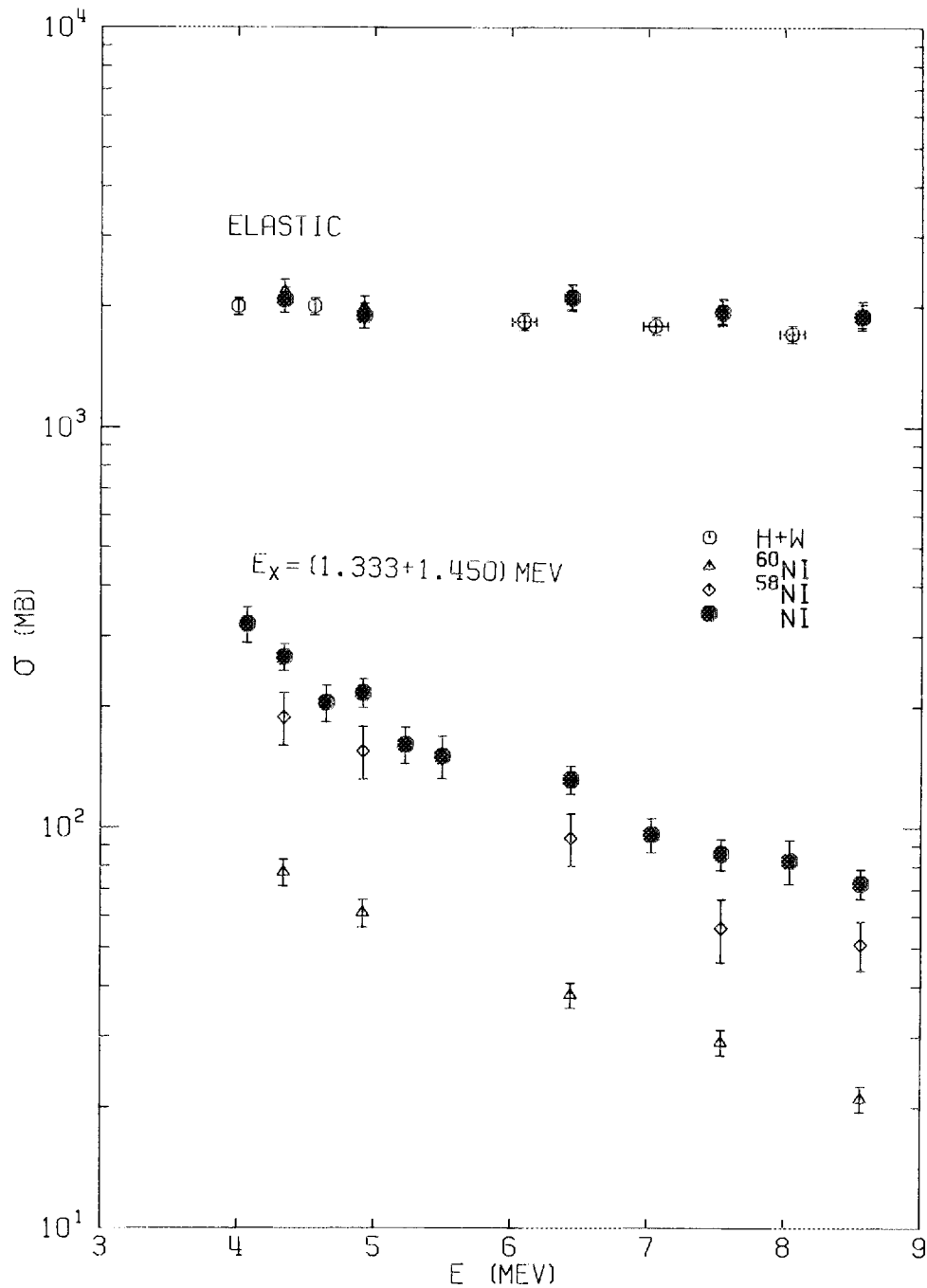


Fig. 12. Our angle-integrated neutron differential cross sections for natural nickel and ^{60}Ni with the Holmqvist and Wiedling (H+W) elastic data.² Our ^{60}Ni elastic results are not evident since they agree well within experimental uncertainties with our natural nickel data. The inelastic data for ^{60}Ni is given per atom of natural nickel. The ^{58}Ni inelastic data, also per atom of natural nickel, was obtained by subtracting the ^{60}Ni inelastic data from the natural nickel inelastic data.

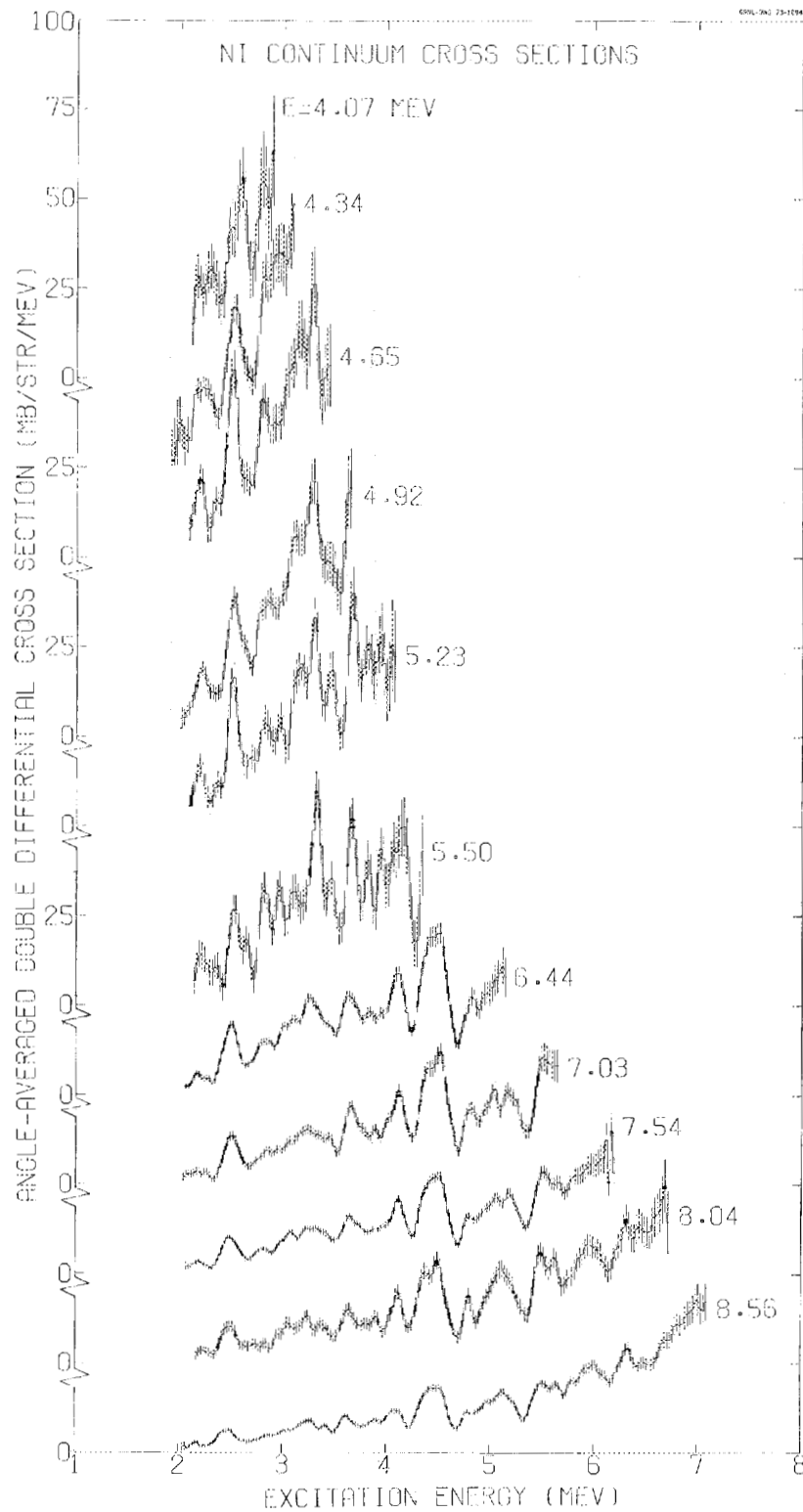


Fig. 13. Natural nickel angle-averaged double-differential cross sections for inelastic scattering to the "continuum" as a function of excitation energy for incident neutron energies, E , from 4.34 to 8.56 MeV.

energy (or to an equivalent out going energy, E') are plotted as a function of the excitation energy for all our energies of measurement. The preferential excitation of the 4^+ levels in ^{58}Ni and ^{60}Ni around 2.5 MeV is clearly seen as is that of the 3^- level in ^{58}Ni at 4.5 MeV. But also there are additional levels or groups of levels which were excited to produce the other structure which is evident.

The adequacy of an evaporation model in describing our inelastic "continua" may be judged from Figure 14 where $\text{SIG}(E \rightarrow E')/E'$ versus E' is plotted where $\text{SIG}(E \rightarrow E') =$ the angle-averaged differential cross section for scattering from incident energy E to exit center-of-mass energy dE' about E' . The straight lines are least squares fits to the data with temperatures resulting from the fits being indicated. The uncertainties on the temperatures are uncertainties in the fitting only. Two fits have been made to each set of data: one covering nearly the entire range in E' for which we extracted data and the other to an E' below which an evaporation model might be more appropriate. The values of E' to which the fits were made are indicated. The fits over the entire range of E' would seem to offer a poor description of the data with there being differences of a factor of 2 among the data and the cross sections given by an evaporation model. Fits over more limited ranges in E' not surprisingly offer a better description of that data to which they are fitted as structure becomes less pronounced with increasing excitation energy (decreasing exit energy E'). As mentioned above, ENDF/B III MAT 1123 describes all inelastic scattering above incident neutron energies of 4 MeV by an evaporation model with a constant temperature of 1 MeV, a number in good agreement with the temperatures resulting from our fits over a limited range in exit energy.

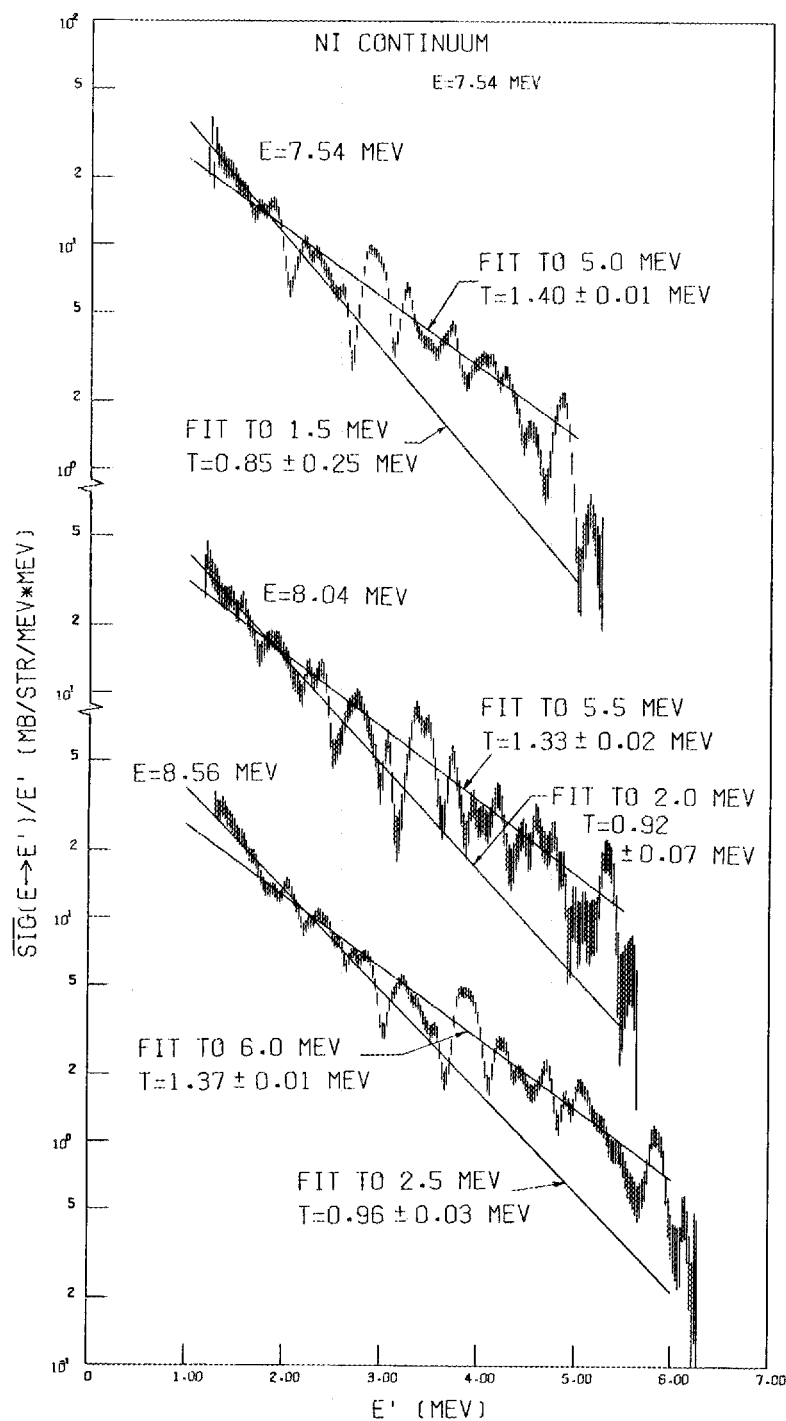


Fig. 14. Natural nickel angle-averaged cross sections for inelastic scattering to the continuum divided by the out-going neutron energy, E' , as a function of out-going neutron energy for incident neutron energies, E , from 7.54 to 8.56 MeV. Least squares fits were made to two different indicated upper limits in E' for each set of data with resulting temperatures, T , being shown. The lower value of E' was equal to the lowest value of the data in all cases.

CONCLUSIONS

Our natural nickel differential elastic scattering cross sections are in agreement with those of Holmqvist and Wiedling in shape though differ slightly in that our shapes change somewhat more than theirs with angle as seen by our uniformly higher Legendre expansion coefficients. Our angle-integrated differential cross sections agree with theirs below 5 MeV but are in the order of 200 mb higher from 6 to 8.56 MeV, a situation similar to that found in comparisons of other data. Our ^{60}Ni differential elastic cross sections are in gratifying agreement with our natural nickel results.

The ENDF/B III MAT 1123 elastic angular distributions are in poor agreement with experimental results from 4 to 8.56 MeV and use a Legendre approximation of order 16 where the highest order required by the experimental data is 9. The ENDF/B III MAT 1123 angle-integrated differential elastic cross sections agree with our results hence are higher than the results of Holmqvist and Wiedling above 6 MeV.

An evaporation model of inelastic scattering to levels of excitation energy in the residual nucleus greater than 6 MeV appears to offer a fair description of inelastic scattering to these levels but becomes questionable in its representation of inelastic scattering to levels of lower excitation energy.

ACKNOWLEDGMENTS

Many have contributed to this experimental program at one time or another and we would like to thank them for their contributions. In particular, we would like to acknowledge the help of J. K. Dickens, J. W. McConnell, J. A. Biggerstaff, A. M. Marusak, P. H. Stelson, C. O. LeRigoleur, and E. Hungerford.

We are deeply indebted to F. C. Maienschein, director of the Neutron Physics Division, for his support of the experiment with the use of computers in report preparation and type setting which produced this report and the other six of our last seven reports.

REFERENCES

1. F. G. Perey and W. E. Kinney, "Carbon Neutron Elastic- and Inelastic- Scattering Cross Sections from 4.5 to 8.5 MeV", ORNL-4441 (December 1970).
F. G. Perey, C. O. LeRigoleur and W. E. Kinney, "Nickel-60 Neutron Elastic- and Inelastic- Scattering Cross Sections from 6.5 to 8.5 MeV", ORNL-4523 (April 1970).
W. E. Kinney and F. G. Perey, "Neutron Elastic- and Inelastic- Scattering Cross Sections from ^{56}Fe in the Energy Range 4.19 to 8.56 MeV", ORNL-4515 (June 1970).
F. G. Perey and W. E. Kinney, "Calcium Neutron Elastic- and Inelastic- Scattering Cross Sections from 4.0 to 8.5 MeV", ORNL-4519 (April 1970).
F. G. Perey and W. E. Kinney, "Sulfur Neutron Elastic- and Inelastic- Scattering Cross Sections from 4 to 8.5 MeV", ORNL-4539 (June 1970).
W. E. Kinney and F. G. Perey, "Neutron Elastic- and Inelastic- Scattering Cross Sections for Co in the Energy Range 4.19 to 8.56 MeV", ORNL-4549 (June 1970).
W. E. Kinney and F. G. Perey, "Neutron Elastic- and Inelastic- Scattering Cross Sections for Mg in the Energy Range 4.19 to 8.56 MeV", ORNL-4550 (June 1970).
W. E. Kinney and F. G. Perey, "Neutron Elastic- and Inelastic- Scattering Cross Sections for Si in the Energy Range 4.19 to 8.56 MeV", ORNL-4517 (July 1970).
F. G. Perey and W. E. Kinney, "Neutron Elastic- and Inelastic- Scattering Cross Sections for Na in the Energy Range of 5.4 to 8.5 MeV", ORNL-4518 (August 1970).
W. E. Kinney and F. G. Perey, "Al Neutron Elastic- and Inelastic- Scattering Cross Sections from 4.19 to 8.56 MeV", ORNL-4516 (October 1970).
F. G. Perey and W. E. Kinney, "V Neutron Elastic- and Inelastic- Scattering Cross Sections from 4.19 to 8.56 MeV", ORNL-4551 (October 1970).
F. G. Perey and W. E. Kinney, "Neutron Elastic- and Inelastic- Scattering Cross Sections for Yttrium in the Energy Range 4.19 to 8.56 MeV", ORNL-4552 (December 1970).
W. E. Kinney and F. G. Perey, "Neutron Elastic- and Inelastic- Scattering Cross Sections for Oxygen in the Energy Range 4.34 to 8.56 MeV", ORNL-4780 (April 1972).
W. E. Kinney and F. G. Perey, "W Neutron Elastic- and Inelastic- Scattering Cross Sections from 4.34 to 8.56 MeV", ORNL-4803 (May 1973).
W. E. Kinney and F. G. Perey, "Natural Titanium Neutron Elastic and Inelastic Scattering Cross Sections from 4.07 to 8.56 MeV", ORNL-4810 (October 1973).
W. E. Kinney and F. G. Perey, "Natural Chromium and ^{52}Cr Neutron Elastic and Inelastic Scattering Cross Sections from 4.07 to 8.56 MeV", ORNL-4806 (to be published).

- F. G. Perey and W. E. Kinney, "Nitrogen Neutron Elastic and Inelastic Scattering Cross Sections from 4.34 to 8.56 MeV", ORNL-4805 (to be published).
- W. E. Kinney and F. G. Perey, "⁵⁴Fe Neutron Elastic and Inelastic Scattering Cross Sections from 4.34 to 8.56 MeV", ORNL-4907 (to be published).
- W. E. Kinney and F. G. Perey "⁶³Cu and ⁶⁵Cu Neutron Elastic and Inelastic Scattering Cross Sections from 5.50 to 8.50 MeV", ORNL-4908 (to be published).
- W. E. Kinney and F. G. Perey, "²⁰⁶Pb, ²⁰⁷Pb, and ²⁰⁸Pb Neutron Elastic and Inelastic Scattering Cross Sections from 5.50 to 8.50 MeV", ORNL-4909 (to be published)
2. B. Holmqvist and T. Wiedling, "Neutron Elastic Scattering Cross Sections Experimental Data and Optical Model Cross Section Calculations", AE-366, Aktiebolaget Atomenergi (1969).
 3. W. E. Kinney, "Neutron Elastic and Inelastic Scattering from ⁵⁶Fe from 4.60 to 7.55 MeV", ORNL-TM-2052, January 1968.
 4. R. E. Textor and V. V. Verbinski, "05S: A Monte Carlo Code for Calculating Pulse Height Distributions Due to Monoenergetic Neutrons Incident on Organic Scintillators", ORNL-4160 (February 1968).
 5. W. E. Kinney, Nucl. Instr. and Methods 83, 15 (1970).
 6. C. Michael Lederer, Jack M. Hollander, and Isadore Perlman, "Tables of Isotopes" Sixth Edition, John Wiley & Sons, Inc. (1967).

APPENDIX

Tabulated Values of Natural Nickel and ^{60}Ni
Neutron Elastic Scattering Cross Sections
and
Cross Sections for Inelastic Scattering
To Discrete Levels

Our measured values for natural nickel and ^{60}Ni neutron elastic scattering and cross sections for inelastic scattering to discrete levels are tabulated below. The uncertainties in differential cross sections, indicated by Δ in the tables, are relative and do *not* include a $\pm 7\%$ uncertainty in detector efficiency which is common to all points. The $\pm 7\%$ uncertainty is included in the integrated and average values. The total cross sections, σ_T , are those we used in the computation of Wick's Limit and were not measured by us.

We have not included the cross sections for inelastic scattering to the continuum. They are available from the National Neutron Cross Section Center, Brookhaven National Laboratory, or from us.

Natural nickel angle-integrated differential cross sections for combined inelastic scattering to the 1.333 MeV level in ^{60}Ni and to the 1.450 MeV level in ^{58}Ni at those energies at which data were taken at only three angles have been corrected for anisotropy in the angular distributions as discussed in the text. The correction was not made to similar ^{60}Ni data hence no integrated values are given for inelastic scattering to the 1.333 MeV level for the ^{60}Ni data in those cases.

Natural nickel cross sections may be found on pages 26 through 31. The cross sections for ^{60}Ni may be found on pages 32 through 36.

NATURAL NICKEL CROSS SECTIONS

$E_n = 4.07 \pm 0.08$ MeV
 (n,n') to: 1.333 MeV Level
 + 1.450 MeV Level

θ_{cm} deg.	$d\sigma/d\omega$ mb/str	Δ (%)	
		+	-
71.15	24.74	19.5	25.6
78.70	24.67	11.1	11.4
86.22	26.75	9.1	14.1

$$\int (d\sigma/d\omega)d\omega = 321.26 \text{ mb} \pm 10.2 \%$$

$E_n = 4.34 \pm 0.07$ MeV
 Elastic Scattering

θ_{cm} deg.	$d\sigma/d\omega$ mb/str	Δ (%)	
		+	-
10.19	1659.29	7.8	9.0
17.80	1544.69	4.6	5.7
17.81	1415.06	10.7	7.2
25.42	1149.57	6.9	5.3
25.42	1104.50	5.3	9.6
25.42	989.67	5.3	5.7
33.03	619.46	6.0	8.9
33.03	837.53	5.5	7.0
40.63	329.92	6.3	7.2
48.22	169.02	7.8	7.2
48.24	184.69	6.8	7.8
55.80	76.01	10.1	10.4
55.81	60.86	14.8	15.5
63.37	27.13	17.2	15.5
63.37	26.14	26.3	19.1
70.92	19.92	25.0	16.4
78.46	27.55	20.0	19.0
85.98	42.18	10.2	9.1
95.98	59.67	10.0	8.8
103.46	62.42	10.8	8.7
110.92	57.21	10.3	8.2
122.34	46.25	9.3	7.5
129.76	35.74	12.3	12.0
137.18	24.43	15.7	10.4

$$\int (d\sigma/d\omega)d\omega = 2076.67 \text{ mb} \pm 7.2 \%$$

$$\text{Wick's Limit} = 1588.95 \text{ mb} \pm 8.1 \%$$

$$\sigma_T = 3.52 \text{ b} \pm 2.0 \%$$

Legendre Fit, Order = 8

k	a_k	Δ (%)
0	330.51318	1.8
1	226.07143	2.2
2	168.84065	2.5
3	125.09531	2.7
4	67.60181	4.1
5	26.00876	8.7
6	9.41905	19.4
7	2.20549	61.9
8	-0.04448	2336.3

$E_n = 4.34 \pm 0.07$ MeV
(n,n') to: 1.333 MeV Level
+ 1.450 MeV Level

θ_{cm} deg.	$d\sigma/d\omega$ mb/str	Δ (%)	
		+	-
25.51	24.33	16.9	22.8
33.15	32.40	11.9	19.3
40.77	24.98	18.7	20.9
48.38	21.99	16.7	16.3
48.41	24.73	14.8	10.9
55.98	23.23	12.0	15.2
55.99	24.46	13.6	10.0
63.57	18.03	18.9	14.7
63.57	20.26	16.4	14.4
71.13	22.70	13.0	17.8
78.67	19.68	16.8	12.5
86.20	19.19	13.8	11.2
96.19	16.75	20.5	16.1
103.67	21.32	17.3	13.4
111.13	18.94	11.9	14.4
122.52	22.69	10.1	11.7
129.93	21.20	11.4	14.4
137.33	18.21	17.5	15.9

$$\int(d\sigma/d\omega)d\omega = 265.51 \text{ mb} \pm 7.8 \%$$

Legendre Fit, Order = 0

k	a_k	Δ (%)
0	42.25774	3.4

$E_n = 4.65 \pm 0.07$ MeV
(n,n') to: 1.333 MeV Level
+ 1.450 MeV Level

θ_{cm} deg.	$d\sigma/d\omega$ mb/str	Δ (%)	
		+	-
71.11	16.87	14.8	12.9
78.65	16.56	12.6	13.9
86.18	15.46	17.1	13.9

$$\int(d\sigma/d\omega)d\omega = 204.24 \text{ mb} \pm 10.5 \%$$

$E_n = 4.92 \pm 0.06$ MeV
Elastic Scattering

θ_{cm} deg.	$d\sigma/d\omega$ mb/str	Δ (%)	
		+	-
10.19	1848.38	4.8	6.4
15.28	1630.60	4.4	6.5
17.81	1476.58	7.4	4.0
22.88	1099.00	7.9	9.1
25.42	984.47	7.1	7.4
25.42	974.62	4.4	4.9
30.50	701.80	6.8	7.1
33.03	618.36	6.4	6.6
40.63	323.78	6.1	5.2
48.23	147.27	5.8	6.7
55.81	50.62	17.0	18.5
63.37	20.14	22.5	19.6
70.94	20.68	38.0	38.0
78.46	31.87	31.8	31.8
85.98	41.66	29.7	29.7
95.98	44.24	10.5	8.3
103.46	42.34	10.6	9.4
110.92	40.83	11.0	6.8
122.34	29.18	12.3	10.0
129.76	21.56	17.7	11.9
137.18	16.10	21.4	14.8

$$\int(d\sigma/d\omega)d\omega = 1897.71 \text{ mb} \pm 7.2 \%$$

$$\text{Wick's Limit} = 1801.30 \text{ mb} \pm 8.1 \%$$

$$\sigma_T = 3.52 \text{ b} \pm 2.0 \%$$

Legendre Fit, Order = 8

k	a_k	Δ (%)
0	302.03101	1.8
1	221.71973	2.0
2	166.72736	2.2
3	123.88963	2.4
4	72.72192	3.4
5	32.75404	6.2
6	12.73978	13.9
7	3.86275	38.0
8	0.86518	104.2

$E_n = 4.92 \pm 0.06$ MeV
 (n,n') to: 1.333 MeV Level
 + 1.450 MeV Level

θ_{cm} deg.	$d\sigma/d\omega$ mb/str	Δ (%)	
		+	-
25.50	28.12	12.5	39.5
33.13	25.45	12.4	21.9
40.75	21.06	13.7	19.9
48.36	19.33	21.6	21.3
55.96	18.36	15.2	17.7
63.53	17.41	16.0	13.5
71.12	20.06	15.1	11.1
78.64	19.39	20.1	23.3
86.16	19.53	14.6	17.8
96.16	12.96	14.6	12.0
103.64	13.89	18.7	10.7
111.10	11.83	15.7	12.5
122.50	16.42	15.8	9.3
129.91	16.30	14.5	18.3
137.30	15.00	14.8	10.0

$$\int(d\sigma/d\omega)d\omega = 216.27 \text{ mb} \pm 8.2 \%$$

Legendre Fit, Order = 3

k	a_k	Δ (%)
0	34.42029	4.2
1	3.10666	34.7
2	1.86345	42.6
3	-0.19829	347.0

$E_n = 5.23 \pm 0.05$ MeV
 (n,n') to: 1.333 MeV Level
 + 1.450 MeV Level

θ_{cm} deg.	$d\sigma/d\omega$ mb/str	Δ (%)	
		+	-
71.08	11.47	18.9	9.1
78.62	13.66	15.3	12.2
86.15	13.66	16.6	13.0

$$\int(d\sigma/d\omega)d\omega = 160.80 \text{ mb} \pm 10.5 \%$$

$E_n = 5.50 \pm 0.05$ MeV
 (n,n') to: 1.333 MeV Level
 + 1.450 MeV Level

θ_{cm} deg.	$d\sigma/d\omega$ mb/str	Δ (%)	
		+	-
48.34	13.33	15.0	17.9
55.94	11.20	18.4	19.0
63.51	11.52	25.8	18.2

$$\int(d\sigma/d\omega)d\omega = 150.39 \text{ mb} \pm 12.3 \%$$

$E_n = 6.44 \pm 0.07$ MeV
Elastic Scattering

θ_{cm} deg.	$d\sigma/d\omega$ mb/str	Δ (%)	
		+	-
15.27	2306.81	4.2	5.6
22.88	1437.00	4.3	5.8
27.96	1030.85	4.8	4.6
35.56	518.87	4.8	5.2
43.17	205.96	6.4	7.6
48.22	122.97	6.6	7.2
55.80	25.03	14.4	14.7
63.37	9.90	21.7	26.9
70.92	20.87	13.7	15.5
78.46	30.80	11.9	10.5
85.98	35.96	8.6	8.0
93.48	32.69	6.9	10.1
100.97	25.64	8.2	9.1
108.44	20.89	9.4	9.6
120.35	12.24	13.8	13.6
127.78	7.13	24.7	22.2
135.20	5.28	33.9	28.4

$E_n = 6.44 \pm 0.07$ MeV
(n,n') to: 1.333 MeV Level
+ 1.450 MeV Level

θ_{cm} deg.	$d\sigma/d\omega$ mb/str	Δ (%)	
		+	-
22.93	24.79	22.2	29.0
28.02	18.80	36.1	11.7
35.64	14.60	37.9	16.7
43.25	12.69	23.4	20.3
48.32	13.71	13.8	17.3
55.91	11.43	13.0	10.4
63.49	9.93	7.1	13.5
71.04	9.46	14.0	11.0
78.59	9.60	13.3	12.7
86.11	10.03	10.4	17.9
93.61	9.12	10.7	13.0
101.10	8.44	10.9	20.1
108.56	9.35	11.8	12.8
120.47	9.53	6.7	19.3
127.89	8.53	15.9	12.5
135.29	8.63	8.2	19.1

$\int(d\sigma/d\omega)d\omega = 2100.94$ mb \pm 7.3 %
Wick's Limit = 2507.46 mb \pm 8.1 %
 $\sigma_T = 3.63$ b \pm 2.0 %

Legendre Fit, Order = 8

k	a_k	Δ (%)
0	334.37500	2.1
1	273.78979	2.3
2	213.88176	2.6
3	159.74303	2.8
4	105.06142	3.4
5	54.79439	4.7
6	23.45544	7.8
7	7.44447	15.1
8	1.87806	34.7

$\int(d\sigma/d\omega)d\omega = 131.76$ mb \pm 8.1 %

Legendre Fit, Order = 3

k	a_k	Δ (%)
0	20.97054	4.0
1	2.73859	26.2
2	1.24954	38.8
3	0.79024	51.2

$E_n = 7.03 \pm 0.06$ MeV
(n,n') to: 1.333 MeV Level
+ 1.450 MeV Level

θ_{cm} deg.	$d\sigma/d\omega$ mb/str	Δ (%)	
		+	-
71.03	8.09	7.6	13.0
78.57	7.37	16.6	16.8
86.09	7.33	10.4	13.9

$\int(d\sigma/d\omega)d\omega = 96.04$ mb \pm 9.8 %

$E_n = 7.54 \pm 0.06$ MeV
Elastic Scattering

θ_{cm} deg.	$d\sigma/d\omega$ mb/str	Δ (%)	
		+	-
15.26	2211.87	4.4	6.1
22.88	1361.96	5.2	5.8
27.96	985.63	4.7	6.0
35.56	450.28	5.2	7.7
43.16	161.90	7.3	7.6
48.22	67.23	10.0	8.4
55.80	9.63	27.5	28.1
63.37	8.54	22.5	24.7
70.92	17.49	14.8	16.3
78.46	25.85	9.1	11.5
85.98	25.54	12.2	12.6
93.48	21.16	11.5	11.3
100.96	16.51	14.0	12.7
108.44	9.56	18.1	19.6
120.35	4.71	30.5	33.3
127.78	2.56	58.2	55.4
135.20	3.15	46.7	47.4

$\int(d\sigma/d\omega)d\omega = 1934.76 \text{ mb} \pm 7.4 \%$
Wick's Limit $= 2729.24 \text{ mb} \pm 8.1 \%$
 $\sigma_T = 3.50 \text{ b} \pm 2.0 \%$

Legendre Fit, Order = 9

k	a_k	Δ (%)
0	307.92749	2.4
1	263.34351	2.6
2	211.95624	2.8
3	161.85159	3.1
4	112.14279	3.6
5	65.06372	4.7
6	31.34418	7.2
7	12.52329	12.6
8	4.09562	24.2
9	0.78223	66.6

$E_n = 7.54 \pm 0.06$ MeV
(n,n') to: 1.333 MeV Level
+ 1.450 MeV Level

θ_{cm} deg.	$d\sigma/d\omega$ mb/str	Δ (%)	
		+	-
35.63	12.31	40.7	24.4
43.24	12.27	16.8	21.9
48.30	8.50	26.3	17.8
55.89	7.98	15.4	12.6
63.46	6.05	12.3	13.5
71.02	7.21	10.4	13.8
78.56	6.35	17.1	19.2
86.08	6.67	11.9	11.4
93.59	7.01	16.8	19.5
101.07	5.95	23.4	22.9
108.54	5.66	19.1	18.0
120.45	5.67	20.4	13.4
127.87	5.30	16.3	21.9
135.28	5.00	15.3	14.2

$\int(d\sigma/d\omega)d\omega = 85.80 \text{ mb} \pm 9.0 \%$

Legendre Fit, Order = 3

k	a_k	Δ (%)
0	13.65548	5.6
1	2.05175	31.9
2	0.58625	77.5
3	0.41234	83.3

$E_n = 8.04 \pm 0.05$ MeV
(n,n') to: 1.333 MeV Level
+ 1.450 MeV Level

θ_{cm} deg.	$d\sigma/d\omega$ mb/str	Δ (%)	
		+	-
71.01	6.87	17.9	14.8
78.55	6.40	29.8	12.4
86.07	6.38	29.5	18.0

$\int(d\sigma/d\omega)d\omega = 82.58 \text{ mb} \pm 12.7 \%$

$E_n = 8.56 \pm 0.05$ MeV
Elastic Scattering

θ_{cm} deg.	$d\sigma/d\omega$ mb/str	Δ (%)	
		+	-
10.18	2772.73	4.4	5.1
15.26	2284.93	4.4	5.3
22.88	1372.74	4.5	7.8
27.95	895.69	4.9	6.1
35.56	376.33	5.7	6.9
43.16	124.19	7.6	10.8
48.22	58.77	8.8	14.9
55.80	6.73	25.8	46.7
63.37	5.82	33.0	37.7
70.92	15.61	13.9	19.0
78.46	18.32	13.7	16.8
85.98	20.43	14.9	13.6
93.48	18.87	7.3	16.6
100.96	14.17	11.5	13.9
108.43	9.47	15.5	20.1
120.35	4.71	32.2	29.3
127.78	3.38	37.4	41.2
135.20	2.54	52.8	52.5

$\int(d\sigma/d\omega)d\omega = 1887.00 \text{ mb} \pm 7.3 \%$
Wick's Limit = 2941.15 mb \pm 8.1 %
 $\sigma_T = 3.41 \text{ b} \pm 2.0 \%$

Legendre Fit, Order = 9

k	a_k	Δ (%)
0	300.32495	2.1
1	260.01099	2.3
2	214.45067	2.4
3	167.13733	2.5
4	119.21698	2.8
5	72.81339	3.6
6	38.81361	5.0
7	18.00531	7.7
8	7.04049	12.4
9	1.93391	24.7

$E_n = 8.56 \pm 0.05$ MeV
(n,n') to: 1.333 MeV Level
+ 1.450 MeV Level

θ_{cm} deg.	$d\sigma/d\omega$ mb/str	Δ (%)	
		+	-
28.00	11.67	22.2	23.1
35.62	11.67	29.2	16.4
43.23	9.70	15.6	18.7
48.29	8.49	21.9	16.3
55.88	6.43	16.0	10.3
63.45	5.72	12.0	19.0
71.00	5.77	14.3	17.4
78.54	5.07	17.1	19.1
86.07	5.42	16.4	13.2
93.57	6.19	14.1	22.0
101.05	5.32	15.5	12.5
108.52	4.98	13.8	14.1
120.43	3.95	19.5	17.5
127.86	3.13	23.2	22.7
135.26	3.89	18.4	18.4

$\int(d\sigma/d\omega)d\omega = 72.46 \text{ mb} \pm 8.5 \%$

Legendre Fit, Order = 3

k	a_k	Δ (%)
0	11.53181	4.8
1	2.36532	18.7
2	0.63234	51.3
3	0.37798	64.9

⁶⁰Ni CROSS SECTIONS

$E_n = 4.07 \pm 0.08$ MeV
(n,n') to: 1.333 MeV Level

θ_{cm} deg.	$d\sigma/d\omega$ mb/str	Δ (%)	
		+	-
71.11	30.52	16.1	8.5
78.66	29.04	11.6	14.8
86.18	27.07	10.6	13.4

$E_n = 4.07 \pm 0.08$ MeV
(n,n') to: 2.158 MeV Level
+ 2.286 MeV Level

θ_{cm} deg.	$d\sigma/d\omega$ mb/str	Δ (%)	
		+	-
71.36	21.36	12.6	19.6
78.91	17.20	13.9	22.6
86.43	19.86	12.1	17.2

Avg. $d\sigma/d\omega = 18.59$ mb/str $\pm 12.7\%$
 $\int(d\sigma/d\omega)d\omega = 233.63$ mb $\pm 12.7\%$

$E_n = 4.07 \pm 0.08$ MeV
(n,n') to: 2.506 MeV Level
+ 2.630 MeV Level

θ_{cm} deg.	$d\sigma/d\omega$ mb/str	Δ (%)	
		+	-
71.54	24.13	13.6	23.7
79.11	22.90	14.0	14.3
86.63	24.95	14.9	16.4

Avg. $d\sigma/d\omega = 23.71$ mb/str $\pm 13.2\%$
 $\int(d\sigma/d\omega)d\omega = 297.90$ mb $\pm 13.2\%$

$E_n = 4.34 \pm 0.07$ MeV
Elastic Scattering

θ_{cm} deg.	$d\sigma/d\omega$ mb/str	Δ (%)	
		+	-
10.18	1954.94	5.9	6.5
17.80	1458.84	5.9	8.3
17.80	1585.83	5.3	5.2
25.41	1087.56	5.8	8.6
25.41	1177.17	4.7	6.7
25.41	1006.88	4.9	6.4
33.02	770.15	5.9	7.2
33.02	639.37	5.1	8.4
40.62	364.12	5.8	7.2
48.21	192.20	7.1	7.8
55.79	72.67	12.1	15.9
63.36	26.07	24.3	23.9
70.90	13.54	35.2	29.4
78.44	28.04	29.3	22.4
85.96	39.51	10.1	10.1
95.96	58.93	7.2	7.4
103.44	61.98	6.5	10.4
110.90	61.58	8.2	9.6
122.32	42.64	10.6	8.8
129.75	35.38	13.6	14.7
137.16	26.59	12.5	12.3

$\int(d\sigma/d\omega)d\omega = 2175.72$ mb $\pm 7.2\%$
Wick's Limit = 1608.14 mb $\pm 8.6\%$
 $\sigma_T = 3.54$ b $\pm 19.0\%$

Legendre Fit, Order = 8

k	a_k	$\Delta(\%)$
0	346.27661	1.8
1	238.59480	2.3
2	182.93558	2.4
3	134.19646	2.9
4	75.43665	4.3
5	30.45334	9.2
6	13.08883	18.0
7	5.32548	30.7
8	1.59220	81.2

$E_n = 4.34 \pm 0.07$ MeV
(n,n') to: 1.333 MeV Level

θ_{cm} deg.	$d\sigma/d\omega$ mb/str	Δ (%)	
		+	-
25.49	35.08	14.5	23.0
33.13	37.63	24.2	23.9
40.75	26.58	17.5	16.8
48.36	24.30	11.4	11.1
55.95	22.40	9.3	8.6
63.53	24.99	13.2	11.8
71.08	25.00	11.5	8.7
78.63	19.63	13.0	16.9
86.15	20.67	10.7	10.8
96.15	23.03	10.0	10.1
103.63	23.44	11.0	13.1
111.09	22.05	13.2	15.6
122.49	24.36	10.5	9.0
129.90	24.43	14.2	9.3
137.30	24.94	10.8	9.4

$$\int(d\sigma/d\omega)d\omega = 295.72 \text{ mb} \pm 7.6 \%$$

Legendre Fit, Order = 0

k	a_k	Δ (%)
0	47.06590	3.1

$E_n = 4.34 \pm 0.07$ MeV
(n,n') to: 2.158 MeV Level
+ 2.286 MeV Level

θ_{cm} deg.	$d\sigma/d\omega$ mb/str	Δ (%)	
		+	-
25.59	17.67	28.0	36.7
33.24	14.13	23.5	31.0
40.88	18.01	22.7	29.6
48.52	27.71	11.7	18.3
56.13	16.36	13.4	16.8
63.72	15.94	19.6	20.8
71.28	14.32	16.9	19.0
78.84	12.60	20.9	13.2
86.36	15.42	14.2	17.0
96.38	17.89	11.8	16.8
103.84	10.74	11.0	26.0
111.30	13.75	17.0	19.5
122.67	15.95	14.8	12.6
130.07	15.11	15.9	16.9
137.45	14.53	15.9	11.5

$$\text{Avg. } d\sigma/d\omega = 14.46 \text{ mb/str} \pm 9.8 \%$$

$$\int(d\sigma/d\omega)d\omega = 181.74 \text{ mb} \pm 9.8 \%$$

$E_n = 4.34 \pm 0.07$ MeV
(n,n') to: 2.506 MeV Level
+ 2.630 MeV Level

θ_{cm} deg.	$d\sigma/d\omega$ mb/str	Δ (%)	
		+	-
25.65	20.55	22.7	29.3
33.34	17.91	22.9	31.0
40.98	18.54	21.6	22.6
48.64	25.33	17.8	32.4
56.26	20.23	17.5	20.0
63.85	13.76	24.0	29.9
71.43	19.52	15.4	26.1
79.00	18.46	12.9	10.7
86.53	14.81	21.4	23.2
96.52	24.08	10.5	21.4
111.44	16.82	13.9	17.2
122.81	19.89	19.0	17.2
130.19	17.46	17.7	17.7
137.55	16.75	16.1	13.9

$$\text{Avg. } d\sigma/d\omega = 17.82 \text{ mb/str} \pm 10.3 \%$$

$$\int(d\sigma/d\omega)d\omega = 223.99 \text{ mb} \pm 10.3 \%$$

$E_n = 4.65 \pm 0.07$ MeV
(n,n') to: 1.333 MeV Level

θ_{cm} deg.	$d\sigma/d\omega$ mb/str	Δ (%)	
		+	-
71.07	18.17	14.3	9.7
78.61	17.27	13.7	10.9
86.14	15.18	13.5	10.5

$E_n = 4.65 \pm 0.07$ MeV
(n,n') to: 2.158 MeV Level
+ 2.286 MeV Level

θ_{cm} deg.	$d\sigma/d\omega$ mb/str	Δ (%)	
		+	-
71.24	9.60	14.5	15.3
78.80	9.33	21.5	21.1
86.32	11.49	18.7	22.9

Avg. $d\sigma/d\omega = 9.82$ mb/str $\pm 13.3\%$
 $\int(d\sigma/d\omega)d\omega = 123.36$ mb $\pm 13.3\%$

$E_n = 4.65 \pm 0.07$ MeV
(n,n') to: 2.506 MeV Level
+ 2.630 MeV Level

θ_{cm} deg.	$d\sigma/d\omega$ mb/str	Δ (%)	
		+	-
71.36	16.89	18.0	19.1
78.92	16.43	15.4	13.6
86.44	15.41	21.5	11.3

Avg. $d\sigma/d\omega = 16.32$ mb/str $\pm 13.0\%$
 $\int(d\sigma/d\omega)d\omega = 205.07$ mb $\pm 13.0\%$

$E_n = 4.92 \pm 0.06$ MeV
Elastic Scattering

θ_{cm} deg.	$d\sigma/d\omega$ mb/str	Δ (%)	
		+	-
10.18	1950.30	4.8	5.6
15.27	1694.91	5.5	7.6
17.80	1496.48	7.5	6.5
22.88	1293.90	4.9	8.4
25.41	965.13	6.9	7.7
25.41	995.88	4.8	4.4
30.49	739.27	6.8	5.9
33.02	627.66	6.0	6.2
40.62	312.51	6.3	6.4
48.21	143.46	6.8	6.1
55.79	44.79	18.2	21.9
63.36	19.65	20.7	21.1
70.91	33.11	15.4	13.6
78.44	43.86	12.2	11.9
85.96	56.62	9.6	7.3
95.96	46.24	13.9	8.3
103.44	45.66	11.3	11.6
110.91	38.71	10.5	10.0
122.32	26.82	13.8	12.1
129.75	18.57	17.5	15.0
137.17	13.70	22.7	13.2

$\int(d\sigma/d\omega)d\omega = 1979.52$ mb $\pm 7.2\%$
Wick's Limit = 1802.51 mb $\pm 8.6\%$
 $\sigma_T = 3.52$ b $\pm 19.0\%$

Legendre Fit, Order = 7

k	a_k	Δ (%)
0	315.05029	1.8
1	229.18994	2.0
2	170.51259	2.3
3	127.33780	2.5
4	79.11858	3.2
5	35.77414	5.6
6	12.38473	11.5
7	2.33064	41.7

$E_n = 4.92 \pm 0.06$ MeV
(n,n') to: 1.333 MeV Level

θ_{cm} deg.	$d\sigma/d\omega$ mb/str	Δ (%)	
		+	-
25.48	19.81	47.2	8.8
33.11	20.92	48.6	10.2
40.73	23.03	13.8	14.8
48.34	22.83	15.7	11.2
55.93	21.52	13.6	11.7
63.52	16.54	15.0	10.2
71.07	22.15	13.9	12.6
78.61	22.62	10.3	7.9
86.13	20.10	16.1	13.1
96.12	16.91	15.1	10.8
103.60	16.51	14.8	12.1
111.06	15.25	24.9	12.7
122.47	16.39	14.9	14.2
129.88	18.80	12.3	12.9
137.28	15.57	15.5	12.1

$$\int(d\sigma/d\omega)d\omega = 234.10 \text{ mb} \pm 7.9 \%$$

Legendre Fit, Order = 0

k	a_k	Δ (%)
0	37.25803	3.6

$E_n = 4.92 \pm 0.06$ MeV
(n,n') to: 2.158 MeV Level
+ 2.286 MeV Level

θ_{cm} deg.	$d\sigma/d\omega$ mb/str	Δ (%)	
		+	-
25.55	12.45	35.3	19.7
33.20	9.44	27.9	24.1
40.84	16.06	20.1	20.3
48.46	12.42	15.9	26.1
56.07	12.10	13.8	17.9
63.68	11.00	22.3	23.6
71.23	13.28	20.8	19.9
78.78	13.30	17.8	24.6
86.31	13.50	12.4	23.9
96.29	8.93	21.2	18.7
103.77	9.02	28.6	18.2
111.22	10.78	12.9	20.0
122.60	9.60	16.4	16.0
130.01	11.47	17.9	17.4
137.39	12.20	20.9	16.0

$$\text{Avg. } d\sigma/d\omega = 11.17 \text{ mb/str} \pm 9.7 \%$$

$$\int(d\sigma/d\omega)d\omega = 140.33 \text{ mb} \pm 9.7 \%$$

$E_n = 4.92 \pm 0.06$ MeV
(n,n') to: 2.506 MeV Level
+ 2.630 MeV Level

θ_{cm} deg.	$d\sigma/d\omega$ mb/str	Δ (%)	
		+	-
25.60	11.27	35.9	16.6
33.26	12.22	23.7	17.2
40.91	13.93	17.2	22.5
48.54	20.40	11.1	19.2
56.16	15.48	20.4	20.6
63.78	14.43	15.5	18.5
71.34	18.10	19.4	32.4
78.89	17.56	18.6	13.5
86.43	17.49	14.9	15.0
96.40	15.32	19.1	16.1
103.88	15.65	12.2	13.0
111.33	13.87	13.3	16.9
122.70	15.37	13.6	15.4
130.09	13.31	14.8	9.8
137.47	12.38	20.7	23.3

$$\text{Avg. } d\sigma/d\omega = 14.84 \text{ mb/str} \pm 9.8 \%$$

$$\int(d\sigma/d\omega)d\omega = 186.46 \text{ mb} \pm 9.8 \%$$

$E_n = 5.23 \pm 0.05$ MeV
(n,n') to: 1.333 MeV Level

θ_{cm} deg.	$d\sigma/d\omega$ mb/str	Δ (%)	
		+	-
71.05	15.18	11.4	10.9
78.59	14.49	17.1	12.6
86.11	16.64	9.9	11.5

$E_n = 5.50 \pm 0.05$ MeV
(n,n') to: 2.158 MeV Level
+ 2.286 MeV Level

θ_{cm} deg.	$d\sigma/d\omega$ mb/str	Δ (%)	
		+	-
48.42	7.19	26.7	21.8
56.02	6.41	24.5	23.5
63.61	7.91	17.6	15.3

Avg. $d\sigma/d\omega = 7.33$ mb/str $\pm 14.0\%$
 $\int(d\sigma/d\omega)d\omega = 92.09$ mb $\pm 14.0\%$

$E_n = 5.23 \pm 0.05$ MeV
(n,n') to: 2.158 MeV Level
+ 2.286 MeV Level

θ_{cm} deg.	$d\sigma/d\omega$ mb/str	Δ (%)	
		+	-
71.19	9.26	16.3	17.3
78.74	8.05	20.8	26.3
86.26	8.42	11.4	18.6

Avg. $d\sigma/d\omega = 8.52$ mb/str $\pm 11.6\%$
 $\int(d\sigma/d\omega)d\omega = 107.09$ mb $\pm 11.6\%$

$E_n = 5.50 \pm 0.05$ MeV
(n,n') to: 2.506 MeV Level
+ 2.630 MeV Level

θ_{cm} deg.	$d\sigma/d\omega$ mb/str	Δ (%)	
		+	-
48.48	11.66	20.1	24.9
56.09	9.54	28.4	22.3
63.68	10.73	19.2	13.0

Avg. $d\sigma/d\omega = 10.66$ mb/str $\pm 13.2\%$
 $\int(d\sigma/d\omega)d\omega = 134.01$ mb $\pm 13.2\%$

$E_n = 5.23 \pm 0.05$ MeV
(n,n') to: 2.506 MeV Level
+ 2.630 MeV Level

θ_{cm} deg.	$d\sigma/d\omega$ mb/str	Δ (%)	
		+	-
71.28	13.72	13.1	11.2
78.83	13.10	15.1	15.1
86.36	12.35	12.7	25.5

Avg. $d\sigma/d\omega = 13.07$ mb/str $\pm 10.8\%$
 $\int(d\sigma/d\omega)d\omega = 164.26$ mb $\pm 10.8\%$

$E_n = 5.50 \pm 0.05$ MeV
(n,n') to: 1.333 MeV Level

θ_{cm} deg.	$d\sigma/d\omega$ mb/str	Δ (%)	
		+	-
48.32	16.06	25.0	13.0
55.91	13.79	19.6	18.8
63.49	13.28	18.9	10.4

ORNL-4807
 UC-79d – Physics
 (ENDF-198)

INTERNAL DISTRIBUTION

- | | | | |
|--------|--|--------|-----------------------------|
| 1-3. | Central Research Library | 47-48. | F. C. Maienschein |
| 4. | ORNL - Y-12 Technical
Library Document
Reference Section | 49. | G. L. Morgan |
| 5-24. | Laboratory Records
Department | 50. | F. R. Mynatt |
| 25. | Laboratory Records,
ORNL R.C. | 51. | E. M. Oblo |
| 26-28. | L. S. Abbott | 52. | R. W. Peelle |
| 29. | R. G. Alsmiller, Jr. | 53. | S. K. Penny |
| 30. | C. E. Clifford | 54-68. | F. G. Perey |
| 31. | F. L. Culler | 69. | R. W. Roussin |
| 32. | J. K. Dickens | 70. | M. J. Skinner |
| 33. | C. Y. Fu | 71. | A. M. Weinberg |
| 34. | W. O. Harms | 72. | A. Zucker |
| 35. | R. F. Hibbs | 73. | H. Feshbach
(Consultant) |
| 36-45. | W. E. Kinney | 74. | P. F. Fox
(Consultant) |
| 46. | T. A. Love | 75. | C. R. Mehl
(Consultant) |
| | | 76. | H. T. Motz
(Consultant) |

EXTERNAL DISTRIBUTION

- 77-78. USAEC Division of Reactor Research and Development,
Washington, D.C. 20545
79. USAEC-RRD Senior Site Representative, ORNL
80. Research and Technical Support Division, AEC, ORO
- 81-308. Given distribution as shown in TID-4500 under UC-79d,
Liquid Metal Fast Breeder Reactors (Physics)
- 309-368. Technical Information Center for ENDF distribution